



# International Agreement Report

---

## In-Tube Steam Condensation in the Presence of Air

Prepared by

A. Tanrikut/TAEA  
O. Yesin/METU

Turkish Atomic Energy Authority  
Eskisehir Yolu 06530 Ankara, Turkey

Middle East Technical University  
06531 Ankara, Turkey

Office of Nuclear Regulatory Research  
U.S. Nuclear Regulatory Commission  
Washington, DC 20555-0001

June 2000

Prepared as part of  
The Agreement on Research Participation and Technical Exchange  
under the International Code Application and Maintenance Program (CAMP)

Published by  
U.S. Nuclear Regulatory Commission

**AVAILABILITY OF REFERENCE MATERIALS  
IN NRC PUBLICATIONS**

**NRC Reference Material**

As of November 1999, you may electronically access NUREG-series publications and other NRC records at NRC's Public Electronic Reading Room at [www.nrc.gov/NRC/ADAMS/index.html](http://www.nrc.gov/NRC/ADAMS/index.html).

Publicly released records include, to name a few, NUREG-series publications; *Federal Register* notices; applicant, licensee, and vendor documents and correspondence; NRC correspondence and internal memoranda; bulletins and information notices; inspection and investigative reports; licensee event reports; and Commission papers and their attachments.

NRC publications in the NUREG series, NRC regulations, and *Title 10, Energy*, in the Code of *Federal Regulations* may also be purchased from one of these two sources.

1. The Superintendent of Documents  
U.S. Government Printing Office  
P. O. Box 37082  
Washington, DC 20402-9328  
[www.access.gpo.gov/su\\_docs](http://www.access.gpo.gov/su_docs)  
202-512-1800
2. The National Technical Information Service  
Springfield, VA 22161-0002  
[www.ntis.gov](http://www.ntis.gov)  
1-800-553-6847 or, locally, 703-605-6000

A single copy of each NRC draft report for comment is available free, to the extent of supply, upon written request as follows:

Address: Office of the Chief Information Officer,  
Reproduction and Distribution  
Services Section

U.S. Nuclear Regulatory Commission  
Washington, DC 20555-0001

E-mail: [DISTRIBUTION@nrc.gov](mailto:DISTRIBUTION@nrc.gov)

Facsimile: 301-415-2289

Some publications in the NUREG series that are posted at NRC's Web site address [www.nrc.gov/NRC/NUREGS/indexnum.html](http://www.nrc.gov/NRC/NUREGS/indexnum.html) are updated regularly and may differ from the last printed version.

**Non-NRC Reference Material**

Documents available from public and special technical libraries include all open literature items, such as books, journal articles, and transactions, *Federal Register* notices, Federal and State legislation, and congressional reports. Such documents as theses, dissertations, foreign reports and translations, and non-NRC conference proceedings may be purchased from their sponsoring organization.

Copies of industry codes and standards used in a substantive manner in the NRC regulatory process are maintained at—

The NRC Technical Library  
Two White Flint North  
11545 Rockville Pike  
Rockville, MD 20852-2738

These standards are available in the library for reference use by the public. Codes and standards are usually copyrighted and may be purchased from the originating organization or, if they are American National Standards, from—

American National Standards Institute  
11 West 42<sup>nd</sup> Street  
New York, NY 10036-8002  
[www.ansi.org](http://www.ansi.org)  
212-642-4900

The NUREG series comprises (1) technical and administrative reports and books prepared by the staff (NUREG-XXXX) or agency contractors (NUREG/CR-XXXX), (2) proceedings of conferences (NUREG/CP-XXXX), (3) reports resulting from international agreements (NUREG/IA-XXXX), (4) brochures (NUREG/BR-XXXX), and (5) compilations of legal decisions and orders of the Commission and Atomic and Safety Licensing Boards and of Directors' decisions under Section 2.206 of NRC's regulations (NUREG-0750).

**DISCLAIMER:** This report was prepared under an international cooperative agreement for the exchange of technical information. Neither the U.S. Government nor any agency thereof, nor any employee, makes any warranty, expressed or implied, or assumes any legal liability or responsibility for any third party's use, or the results of such use, of any information, apparatus, product or process disclosed in this publication, or represents that its use by such third party would not infringe privately owned rights.



# International Agreement Report

---

## In-Tube Steam Condensation in the Presence of Air

Prepared by

A. Tanrikut/TAEA  
O. Yesin/METU

Turkish Atomic Energy Authority  
Eskisehir Yolu 06530 Ankara, Turkey

Middle East Technical University  
06531 Ankara, Turkey

**Office of Nuclear Regulatory Research  
U.S. Nuclear Regulatory Commission  
Washington, DC 20555-0001**

**June 2000**

Prepared as part of  
The Agreement on Research Participation and Technical Exchange  
under the International Code Application and Maintenance Program (CAMP)

**Published by  
U.S. Nuclear Regulatory Commission**

## ABSTRACT

In this research work, in-tube condensation in the presence of air is investigated experimentally for different operating conditions, and inhibiting effect of air is analyzed by comparing the experimental data of air/steam mixture with the data of corresponding pure steam cases, with respect to temperature, heat flux, air mass fraction, and film Reynolds number. The test matrix covers the range of;  $P_n=2-6$  bars,  $Re_v=45,000-94,000$ , and  $X_i=0\% - 52\%$ . The inhibiting effect of air manifests itself as a remarkable decrease in centerline temperature ( $10\text{ }^\circ\text{C} - 50\text{ }^\circ\text{C}$ ), depending on inlet air mass fraction. However, the measured centerline temperature is suppressed compared to the predicted one, from the Gibbs-Dalton law, which indicates that the centerline temperature measurements are highly affected by inner wall thermal conditions, possibly due to narrow channel and high vapor Reynolds number. Even at the lowest air quality (10 %) the reduction of the local heat flux is 20 % while it reaches up to 50 % for the quality of 40 %. Vapor mass flow rate may dominate over system pressure, concerning the effect on local heat flux, for cases with air/vapor mixture. The situation is rather different in pure vapor runs, that is increase in system pressure has a strong effect on enhancement of predicted, and even measured, wall subcooling degree and hence on increase in local heat flux. The investigation for the effect of superheating of steam on condensation process reveals the fact that inlet superheating of steam has no considerable effect on heat flux. The calculated film Reynolds number decreases as air mass fraction increases at the same system pressure setting, and falls into the range of turbulent region ( $Re_f > 300$ ) for almost all experimental runs. The RELAP5 code overpredicted majority of experimental local heat flux data by 5 % – 50 %.

## TABLE OF CONTENTS

ABSTRACT	iii
TABLE OF CONTENTS	v
NOMENCLATURE	vii
CHAPTER	
1. INTRODUCTION	1
2. DESCRIPTION OF THE TEST FACILITY	3
2.1 Steam/gas Supply	3
2.2 Connecting Piping and Pipe Fittings	4
2.3 Test Section	5
2.3.1 Condenser Tube	5
2.3.2 Jacket Pipe	6
2.4 Instrumentation	7
2.4.1 Thermocouples	7
2.4.2 Pressure Transducer	12
2.4.3 Flowmeter	13
2.5 Data Acquisition System	14
3. OPERATING PROCEDURES OF THE TEST FACILITY	15
3.1 System Check	15
3.1.1 Isothermal Check of Thermocouples	15
3.1.2 Prediction of Environmental Heat Loss	17
3.1.3 Prediction of Fin Effect for Inner Wall Temperature Measurements	17
3.1.4 Reproducibility of Data	20
3.2 Experiments	21
3.2.1 System Start-up	21
3.2.2 Operating at Steady-state Conditions and Data Logging	22
3.2.3 System Shutdown	22
4. EXPERIMENTAL TEST MATRIX	23
5. DATA REDUCTION PROCEDURE	26

<b>6. EXPERIMENTAL RESULTS AND DISCUSSION</b>	<b>30</b>
6.1 Introduction	30
6.2 Temperature Distribution	30
6.3 Local Heat Flux Distribution	37
6.4 Local Air Mass Fraction Distribution	44
6.5 Condensate Film Reynolds Number	46
6.6. Comparison with Theory	47
<b>LIST OF REFERENCES</b>	<b>50</b>
<b>APPENDIX A: PHOTOGRAPHS OF THE METU-CTF</b>	<b>51</b>
<b>APPENDIX B: SPECIFICATIONS OF INSTRUMENTATION                     AND DATA ACQUISITION SYSTEMS</b>	<b>55</b>
<b>APPENDIX C: ERROR ANALYSIS</b>	<b>56</b>

## NOMENCLATURE

### Latin Symbols:

A	Coefficient of exponential fitting expression
A	Area, m <sup>2</sup>
B	Coefficient of exponential fitting expression
c <sub>p</sub>	Specific heat at constant pressure, J/kg·°C
d, D	Diameter, m
h	Convective heat transfer coefficient, W/m <sup>2</sup> ·°C
h	Enthalpy, J/kg
<i>m</i>	Mass flow rate, kg/s
M	Molecular weight
P	Pressure, bar
q	Heat transfer rate, W
q''	Heat flux, W/m <sup>2</sup>
r	Correlation coefficient
Re	Reynolds number
S	Deviation from fitting curve
T	Temperature, °C
x	Axial distance, m
X	Noncondensable gas quality

### Greek Symbols:

α	Flow coefficient
μ	Dynamic viscosity, kg/m·s
ρ	Density, kg/m <sup>3</sup>
σ	Standard deviation

### Subscripts:

cw	Cooling water
D	Based on diameter
h	Hydraulic
i	Inner, inlet
n	Nominal
s	Saturation
t	Total
v	Vapor phase
w	Wall

## CHAPTER 1

### INTRODUCTION

The introduction of nuclear power becomes an attractive solution to the problem of increasing demand for electricity power capacity in Turkey. Thus, Turkey is willing to follow the technological development trends in advanced reactor systems. A part of our long-term research and development efforts is planned to concentrate on passive cooling systems. The primary objectives of the passive design features are to simplify the design, which assures the minimized demand on operator, and to improve plant safety. The research on passive systems mainly comprises the computer code assessment studies and includes the applications for both old and new generation reactor systems. To accomplish these features the operating principles of passive safety systems should be well understood by an experimental validation program. Such a validation program is also important for the assessment of advanced computer codes, which are currently used for design and licensing procedures. The condensation mode of heat transfer plays an important role for the passive heat removal applications in the current nuclear power plants (e.g. decay heat removal via steam generators in case of loss of heat removal system) and advanced water-cooled reactor systems. But it is well established that the presence of noncondensable gases can greatly inhibit the condensation process due to the build-up of noncondensable gas concentration at the liquid/gas interface. The isolation condenser of passive containment cooling system of the simplified boiling water reactors is a typical application area of in-tube condensation in the presence of noncondensable. The research work concerning the application of condensation in the presence of air, as a noncondensable gas, was first undertaken for a Once Through Steam Generator (OTSG) type of PWR for which experimental data were available. These experimental data were obtained from the 2X4 test loop of the University of Maryland at College Park (UMCP), addressing a very important safety issue called the loss of residual heat removal system after reactor shutdown. The experimental data were used for the assessment of RELAP5/mod3 (v5m5) thermal-hydraulic computer code and both the effect of Nusselt model, incorporated in the code as the condensation model, and the effect of nodalization model were investigated [1].

But the lack of measurements for the inside of the steam generator has led us to the conclusion that the separate effect test is strongly needed for the investigation of in-tube condensation and the effect of noncondensables on the condensation mode of heat transfer. Thus, an experimental study which could enable us for the fundamental investigation of condensation in the presence of air was planned in cooperation with the Mechanical Engineering Department of the Middle East Technical University (METU), Ankara, in the frame of a project (Project No: 94403507) between the Turkish Atomic Energy Authority (TAEA) and METU. The project is partially sponsored by the International Atomic Energy Authority (IAEA) under the Coordinated Research Program (Contract No: 8905/R0) which is entitled *"Thermohydraulic Relationships for Advanced Water Cooled Reactors"*.

The experimental program [2] covers a wide range of steam and air/steam mixture flow rates under forced convection conditions –which partly falls outside the range encountered in typical passive heat removal applications in NPPs due to high Reynolds number– and has the purpose to investigate the inhibiting effect of air on steam condensation process. The results of this experimental study are also planned to be supplementary in nature for other experimental investigations such as those performed at the Massachusetts Institute of Technology (MIT), Cambridge, and University of California, Berkeley, (UCB). These investigations undertaken at MIT and UCB aim to support GE's Passive Containment Cooling System (PCCS) and Isolation Condenser (IC) designs, with relatively lower Reynolds number.

As stated in the CAMP (Thermalhydraulic Code Applications and Maintenance Program) agreement between the Turkish Atomic Energy Authority (TAEA) and the US Nuclear Regulatory Commission (USNRC), the experimental data on in-tube steam condensation in the presence of air are opened to the USNRC. The data will be utilized for the assessment and validation of the RELAP5/mod3 thermal-hydraulic system analysis code. The assessment of this computer code, based on the data of MIT and UCB for pure steam condensation and condensation in the presence of air and helium was finished. [3].

## CHAPTER 2

### DESCRIPTION OF THE TEST FACILITY

The test facility, named as METU Condensation Test Facility (METU-CTF), was installed at the Mechanical Engineering Department of the Middle East Technical University (METU). The photographs of the facility are presented in Appendix A. The experimental apparatus consisting of an open steam or steam/gas system and an open cooling water system is depicted in the flow diagram of Figure 2.1. The details of the apparatus are described in the following Sections:

#### 2.1 Steam/gas Supply

Steam is generated in a boiler (1.6 m high, 0.45 m ID) by using four immersion type sheathed electrical heaters. Three of these heaters have a nominal power of 10 kW each and the fourth one has a power of 7.5 kW, at 380 V. All the heaters can be individually controlled by switching on or off. One of these heaters, i.e. the one with 7.5 kW power, is connected to a variac for continuous control of power.

The boiler tank was designed to withstand an internal pressure of 15 atm (at  $T=20\text{ }^{\circ}\text{C}$ ) and was tested at this pressure. The maximum operating pressure of the tank is 10 atm. To ensure dry steam at the exit of the boiler, a mechanical separator directly connected to the exit nozzle was installed. However, electrical pre-heating with three heaters (0.5 kW per heater) is also available at the entrance of the test section to increase the temperature of steam, so that steam is guaranteed to be 100% dry. The boiler tank was thermally insulated to reduce environmental heat loss.

Compressed air can be supplied either to the boiler tank (directly to the water) or to the steam line via a nozzle (after the orifice meter) on the horizontal part of the pipe which connects the boiler and the test section. Preference was given to the first method; i.e. injection to the boiler, during most of the experiments since system behavior is more stable compared

to the second method, when air mass flow rate is increased. When air injection was performed by the second method (to the horizontal piping), air injected passes through the preheating section so that local steam condensation was avoided at the entrance of the test section due to thermal inequilibrium of steam and air. The air supply system consists of an air compressor and three compressed air tanks with a total capacity of 600 liters. The maximum pressure of the compressed air system is 10 bars.

The boiler tank is equipped with the measuring instruments given below;

- level gauge with an operating pressure of 16 bars and a test pressure of 32 bars,
- safety vent valve of spring lift type with an operating pressure of 12 bars,
- pressure controller for cutting the power off at a predetermined maximum pressure setting,
- pressure gauge (1–16 bars),
- relief valve (19.05 mm ID).

## **2.2 Connecting Piping and Pipe Fittings**

The pipe connecting the boiler tank and the test section has a length of approximately 2 m and an ID of 38.1 mm. The pipe was connected to the boiler tank via an isolation valve. This isolation valve (38.1 mm ID) is used to isolate the boiler until inside pressure of the tank is increased to a pre-determined level. The measurements performed on this part of the experimental facility are mass flow rate via a differential pressure transmitter and temperature. There are three electric heaters (0.5 kW each at 220 V) installed to the horizontal part of the piping between the orifice meter and the test section. The pipe connecting the boiler and the test section was thermally insulated.

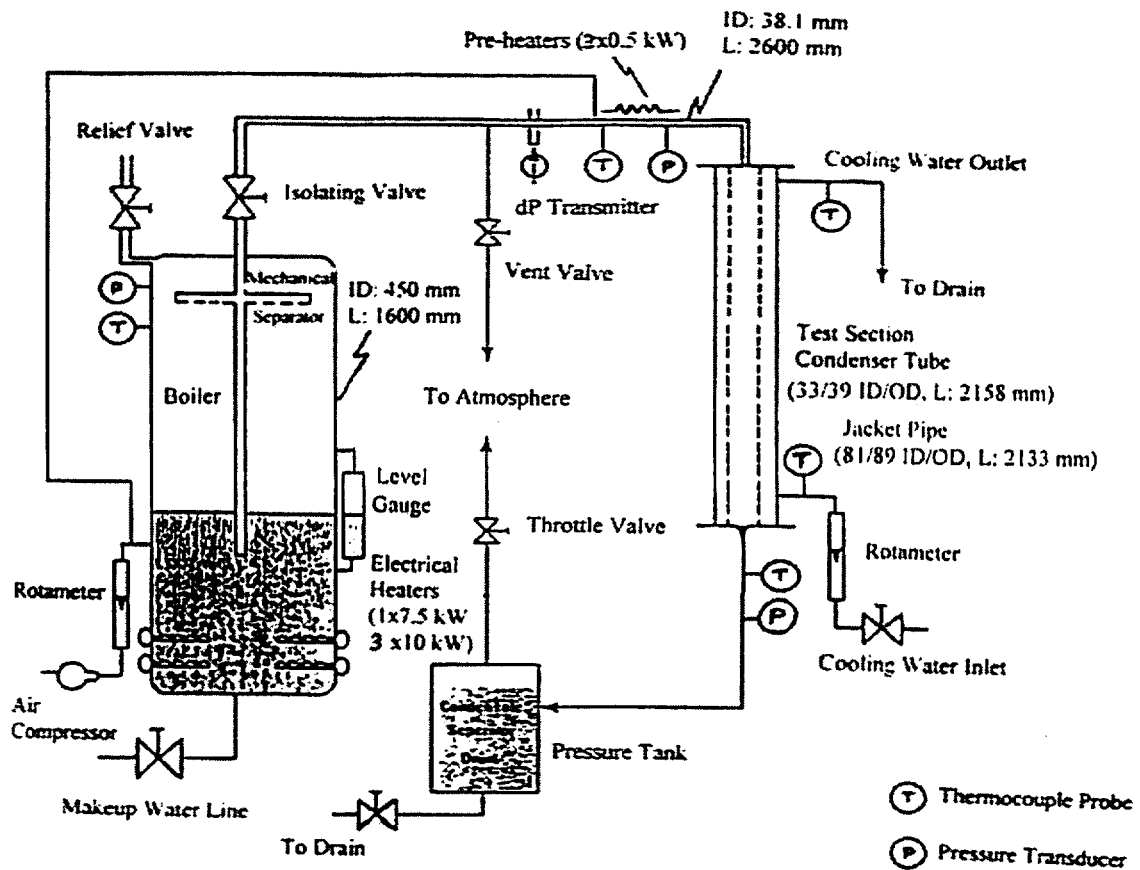


Figure 2.1. The Flow Diagram of the METU-CTF

### 2.3 Test Section

The test section is a heat exchanger of countercurrent type, that is steam or steam/gas mixture flows downward inside the condenser tube (inner tube) and cooling water flows upward inside the jacket pipe (outer pipe).

#### 2.3.1 Condenser Tube

The condenser tube consists of a 2.15 m long seamless stainless steel tube with 33/39 mm ID/OD and is flanged at both ends with sealing materials. The condenser tube was flanged to the inlet (33.5/42.6 mm ID/OD) and exit (33.5/42.6 mm ID/OD) pipes of the test

section. The total length of the inlet pipe from the horizontal part of the pipe section down to the condenser tube is approximately 33 cm ( $10 \times d_i$ , where  $d_i$  is the inner diameter of the tube) and this length is long enough for the mixture flow to become fully developed before entering the condenser. It should also be noted that some uncertainties (such as irregular film development or dropwise condensation) associated with the liquid film development at the entrance of the condenser tube are expected to occur in this development region since the entrance region was not thermally insulated. A pressure measurement port was located at the vertical part of the inlet pipe flanged to the condenser tube.

A total of 13 holes (1.5 mm diameter) were drilled with an angle of  $30^\circ$  at different elevations along the condenser tube length to fix the thermocouples for inner wall temperature measurements. The condenser tube was tested at 10 atm pressure to check that inner wall of the tube was not pierced during the drilling process.

The outlet of the condenser tube is connected to a tank via exit part of the test section. This tank is used to keep the system pressure at a constant level by controlling the flow rate of steam or air/steam mixture through a valve connected to the tank. The measured parameters at the exit of the test section are pressure and temperature.

### **2.3.2 Jacket Pipe**

The jacket pipe surrounding the condenser tube is made of sheet iron and has a length of 2.133 m and 81.2/89 mm ID/OD. The cooling water is supplied via a nozzle which has been welded on the jacket pipe. Similarly, cooling water outlet consists of a nozzle which is connected to the building water discharge system. Inner diameter of all these nozzles is 12.7 mm. A total of 15 holes (1.5 mm diameter) were drilled radially at different elevations for installation of the thermocouples to be used for cooling water temperature measurements. The measured cooling water temperature is used to determine heat flux profile along the annulus region. The jacket pipe was thermally insulated to reduce environmental heat losses.

## **2.4 Instrumentation**

The details of the technical features of the equipment are given in Appendix B.

### **2.4.1 Thermocouples**

Thirteen thermocouples were inserted into the holes which have been drilled on the outer surface of the stainless steel condenser tube with an angle of  $30^\circ$  and soldered by silver. The distance between the inner wall and the tips of thermocouples is approximately 0.5 mm. (Figure 2.2)

Fifteen thermocouples were inserted into the holes, drilled on the outer surface of the jacket pipe, and fixed by compression fittings sealed by Teflon material. Thirteen of these thermocouples are at the same elevation as the thermocouples to be used for inner wall temperature measurements. Besides this, two additional thermocouples were inserted at the same elevation but at a  $180^\circ$  offset orientation. The purpose of these two additional temperature measurements is to observe the angular variation of the cooling water temperature.

Ten thermocouples were fixed to a 2 mm diameter Inconel guide wire and installed at the central position of the condenser tube for the central temperature measurements. The guide wire was fixed at both ends of the test section.

The installation locations of all thermocouples are given in Figure 2.3.

Inner Wall of  
Condenser Tube

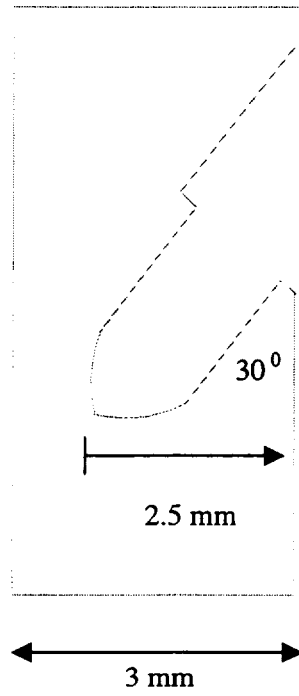


Figure 2.2. Inner Wall Measurement Technique



All thermocouples for inner wall and cooling water temperature measurements are of L-type (Fe-Const type designed according to DIN Standard) and sheathed by Inconel material. The thermocouples used for condenser tube central temperature measurements are of J-type (Fe-Const type designed according to USA standards) and these thermocouples have a temperature-voltage relation very similar to those of L-type thermocouples. The nominal outside diameter and wire diameter of all sheathed thermocouples is approximately 1.5 mm and 0.3 mm, respectively. The precision of this type of thermocouples, which belong to second tolerance class according to the standard IEC 584-2, is  $\pm 2.5$  °C between  $-40$  °C and  $333$  °C.

The deviation of each thermocouple measurement as compared with the mercury thermometer and T-type thermocouple (manufactured by OMEGA) measurements is given in Figs. 2.4–2.7 for  $T_n=50$  °C,  $97$  °C,  $150$  °C and  $180$  °C, respectively. As a result of these comparisons, maximum deviations from reference measurement are found to be  $-0.82\%$ ,  $-1.16\%$ ,  $-1.13\%$  and  $+0.83\%$  for nominal temperature settings of  $50$  °C,  $97$  °C,  $150$  °C and  $180$  °C, respectively.

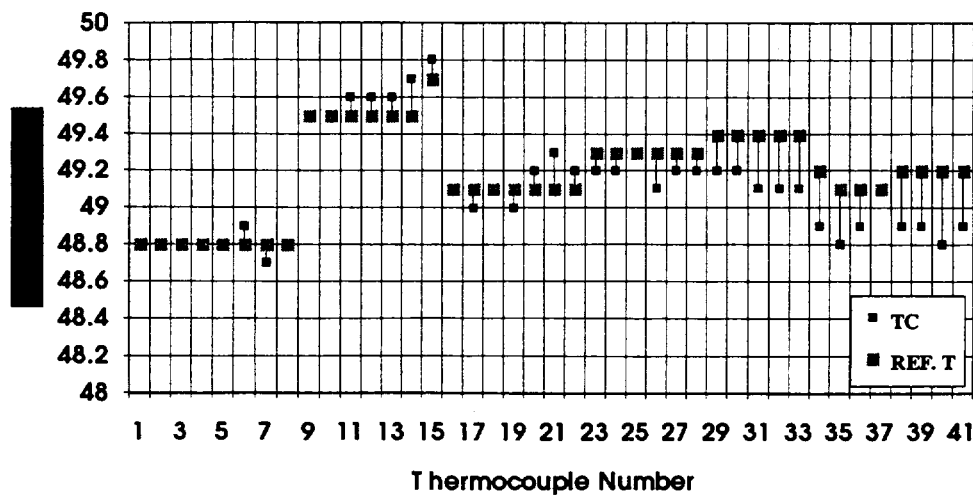


Figure 2.4. Comparison of Thermocouple and Reference Temperature Measurements at  $T_n=50$  °C (Water)

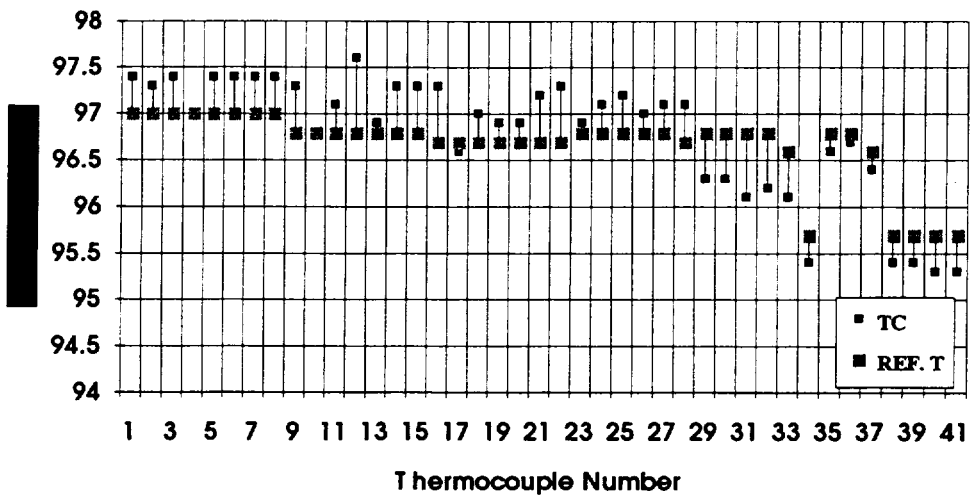


Figure 2.5. Comparison of Thermocouple and Reference Temperature Measurements at  $T_n=97\text{ }^\circ\text{C}$  (Water)

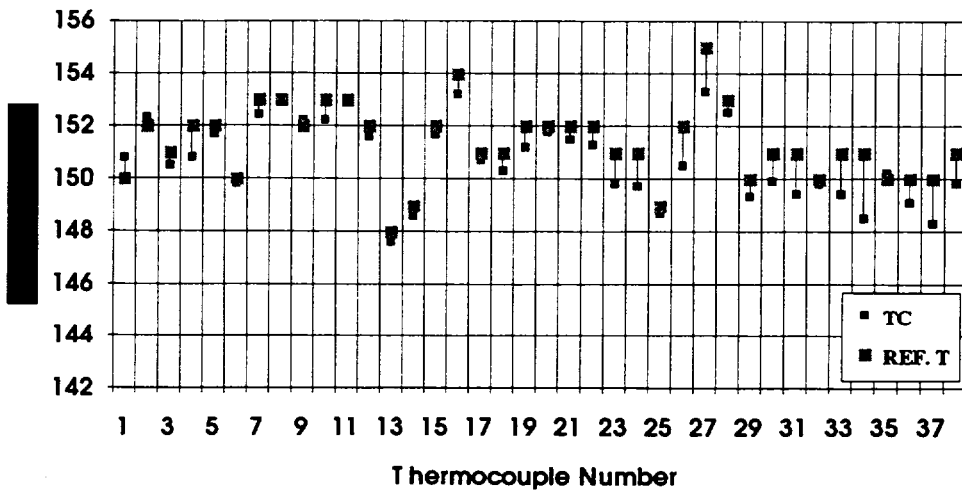


Figure 2.6. Comparison of Thermocouple and Reference Temperature Measurements at  $T_n=150\text{ }^\circ\text{C}$  (Air)

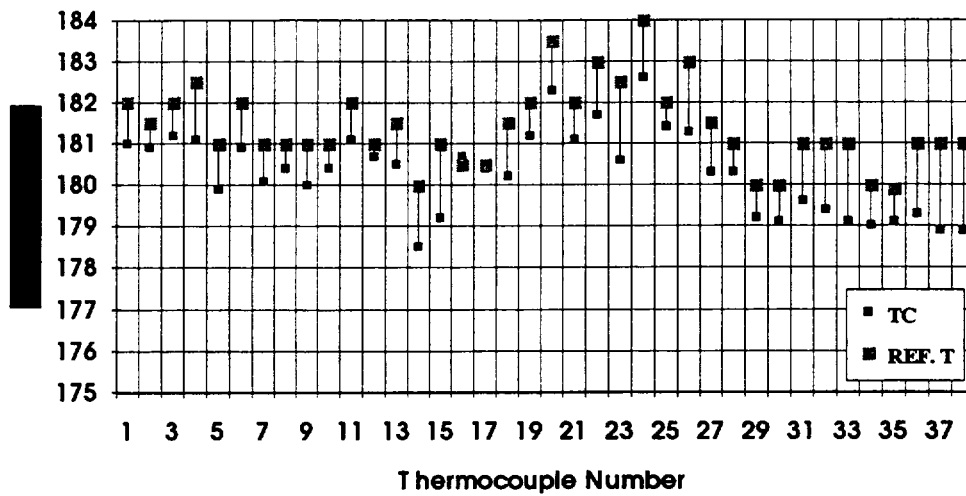


Figure 2.7. Comparison of Thermocouple and Reference Temperature Measurements at  $T_n=180\text{ }^\circ\text{C}$  (Air)

### 2.4.2 Pressure Transducer

A strain gauge type pressure transducer (product of Transinstruments Inc.), installed at the entrance of the test section, can be used for pressure measurement in the interval of 0–6 bars (g) and has an output of 4–20 mA. The power supply of the transmitter is 24V DC. The calibration of this transmitter was made by using air as the operating medium and the result of this calibration is shown in Figure 2.8.

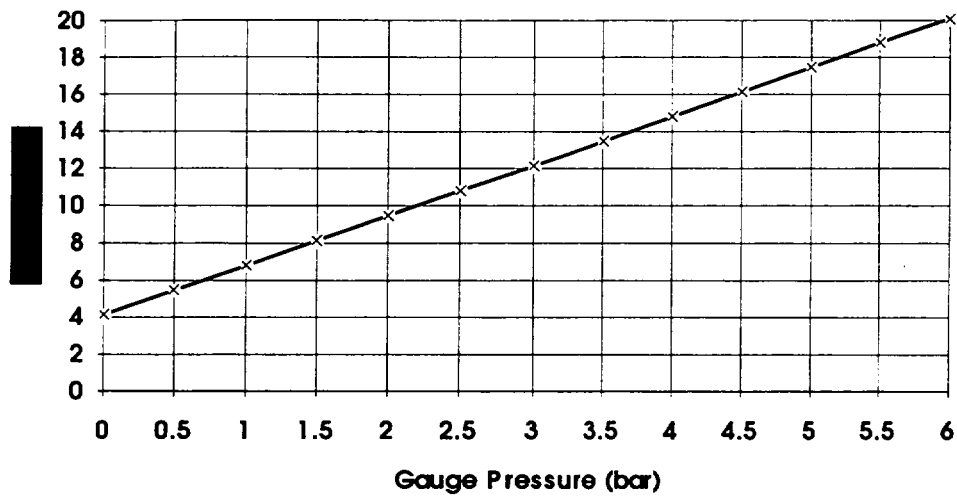


Figure 2.8. The Calibration Relation of the Pressure Transducer

### 2.4.3 Flowmeter

The flow rate measurement of steam is performed by the differential pressure transmitter which is the product of ABB Kent-Taylor Company. The device produces current in the range of 4–20 mA corresponding to the differential pressure range of the transmitter which is 11.7–70 kPa. The current output of the device is linear with respect to differential pressure.

Three types of orifices with flow diameters of 6, 10 and 12.5 mm were calibrated by using water as operating medium and flow coefficients, as a function of Reynolds number, were obtained. The characteristics of the orifice (flow diameter: 12.5 mm) used in the experiments is shown in Figure 2.9. The data obtained during calibration was fitted using the following relation:

$$\alpha = 0.2 * \ln(\text{Re}) - 1.458 \quad (2.1)$$

where  $\alpha$  is the flow coefficient and Re is Reynolds number.

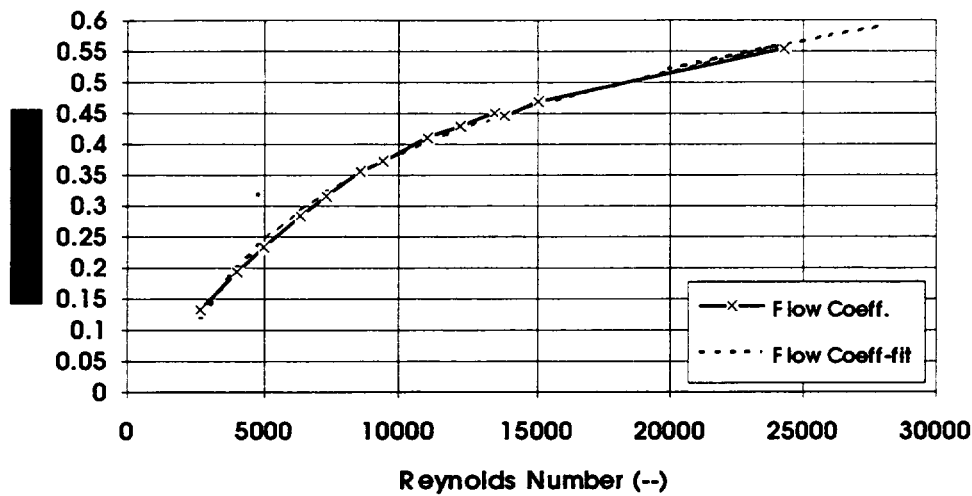


Figure 2.9. The Characteristics of the Orifice with the Diameter of 12.5 mm

### 2.5 Data Acquisition System

The data acquisition system consists of one multifunctional analog and digital I/O card (data acquisition card, PCL-812PG), three programmable amplifier and channel multiplexing daughter board (PCLD-889) for the analog input channels of the data acquisition card which have a total of 48 channels, and an IBM-486 computer system. The data acquisition card and multiplexers are the products of Advantech Co., Ltd, and technical details are given in Appendix A.

Total of 40 thermocouple wires was mounted on the multiplexing daughter cards. The temperatures were continuously monitored on the colour monitor during experiments. The GENIE software was installed to read, display, and log data to disk. The GENIE software, which is the product of Advantech Co., Ltd., is designed to run in the Microsoft Windows 95 environment. GENIE provides an intuitive object oriented graphical use interface that simplifies control strategy and display setups. The user can design his own strategy for controlling signals during experiments or any kind of industrial process.

## CHAPTER 3

### OPERATING PROCEDURES OF THE TEST FACILITY

The operating procedure of the METU-CTF consists of two main stages: system check and experiments. The former stage is important to understand the response of thermocouples at certain operating conditions and to estimate the rate of environmental heat losses. The second stage includes system start-up, data logging and system shutdown.

#### 3.1 System Check

##### 3.1.1 Isothermal Check of Thermocouples

The isothermal check of the thermocouples was done at various temperature levels. The results of these two tests are given in Table 3.1. The first test ( $T \sim 20 \text{ }^\circ\text{C}$ ) was performed with stagnant water while the second one ( $T \sim 110 \text{ }^\circ\text{C}$ ) was under high flow rate ( $1.72 \times 10^{-2} \text{ kg/s}$ ) and high pressure ( $P \sim 1.4 \text{ bars}$ ) conditions. In the second test, steam and two-phase flow was established in the condenser tube and jacket pipe, respectively. Apart from the isothermal check of the thermocouples, the second test has also shown that the centrally located thermocouples were operating properly, at least in the range of thermocouple tolerances, when the saturation temperature ( $T \sim 110 \text{ }^\circ\text{C}$ ) was concerned.

Table 3.1. Data Collected in the Isothermal Check of Thermocouples

TC No	TC Code	Temperature (°C)	
1	TC-1	19.4	
2	TC-2	19.8	111.5
3	TC-3	19.5	110.7
4	TC-4	19.9	110.3
5	TC-5	19.9	109.7
6	TC-6	19.9	111.6
7	TC-7	19.5	112.4
8	TC-8	19.9	110.3
9	TC-9	19.5	110.7
10	TC-10	19.5	109.8
11	TC-11	19.9	109.4
12	TW-1	17.6	106.7
13	TW-2	17.9	107.9
14	TW-3	18.0	105.3
15	TW-4	18.0	109.3
16	TW-5	18.5	108.5
17	TW-6	18.5	109.8
18	TW-7	18.5	107.0
19	TW-8	18.5	108.9
20	TW-9	18.0	109.8
21	TW-10	18.5	109.3
22	TW-11	18.5	109.7
23	TW-12	18.0	110.3
24	TW-13	18.5	109.8
25	TJ-1	16.6	104.0
26	TJ-2	16.5	104.4
27	TJ-3	16.1	105.8
28	TJ-4	16.1	104.9
29	TJ-5	17.1	105.3
30	TJ-6	17.1	104.0
31	TJ-7		104.3
32	TJ-8	15.1	103.5
33	TJ-9		106.1
34	TJ-10	16.6	103.4
35	TJ-11	15.6	103.5
36	TJ-12	16.1	
37	TJ-13		104.3
38	TJ-4R	15.7	104.8
39	TJ-12R		104.0

Notes: TC: central thermocouple

TW: wall thermocouples

TJ: jacket thermocouples

R extension stands for thermocouple at the reverse side  
of the one with the same number

### 3.1.2 Prediction of Environmental Heat Loss

The effect of environmental heat loss on measurements was tested by water under stagnant conditions. Both sides of the test section were filled with hot water fed directly from the boiler. The data collection duration was 422 s. As can be seen in Figure 3.1, insulation of the test section is effective so that rate of temperature decrease was measured to be  $\sim 0.007$  °C/s which yields a maximum heat loss of about 0.1 kW at this operating condition

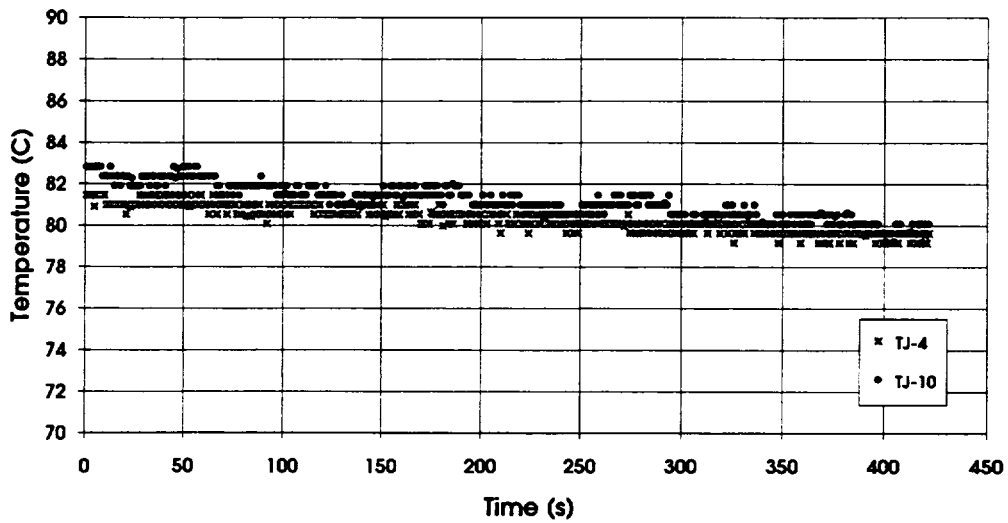


Figure 3.1. Effect of Environmental Heat Loss on Temperature Measurements in Jacket Pipe (TJ-4 at 80 cm and TJ-10 at 180 cm, from bottom of test section,  $T_{env} \sim 17.6$  °C)

### 3.1.3 Prediction of Fin Effect for Inner Wall Temperature Measurements

As described in Sub-section 2.4.1, inner wall temperature measurements were performed by thirteen thermocouples inserted into the holes which have been drilled on the outer surface of the condenser tube with an angle of 30° and soldered by silver. The sheathed thermocouple wires are passing through the jacket pipe so that the inner wall temperature measurements could be affected by local cooling water temperature by a possible fin effect.

A test was performed by filling the condenser tube with stagnant water ( $T_c=80\text{ }^\circ\text{C}$ ) and by keeping the cooling water ( $T_i=17\text{ }^\circ\text{C}$ ) flowing through the jacket pipe at a rate of about 0.25 kg/s. The flow rate was kept close to the cooling water flow rate values given in the test matrix (Chapter 4). The reason for keeping the hot water stagnant inside the condenser tube was to check the difference between the bulk and inner wall temperatures. It was expected that the difference would be small if fin effect was not dominant. The test result is presented in Figure 3.2. It is seen that the temperature difference is about 8 °C and 4 °C at 20 s and 160 s, respectively. It is clear that the difference is more at the beginning of the transient process during which the system temperature is high. It should also be noted that a temperature profile could develop in radial direction due to local natural convection currents so that the measured temperature difference between centerline and inner wall seems reasonable. To support this, the wall temperature at exactly the same radial distance from the inner surface (0.5 mm) is also predicted by the RELAP5/mod3 thermal-hydraulic system analysis computer code [4] by imposing the same test boundary conditions, and as illustrated in Figure 3.3, the discrepancy was small ( $\pm 2\text{ }^\circ\text{C}$ ). Because of this reason, no correction was made for the inner wall measurements.

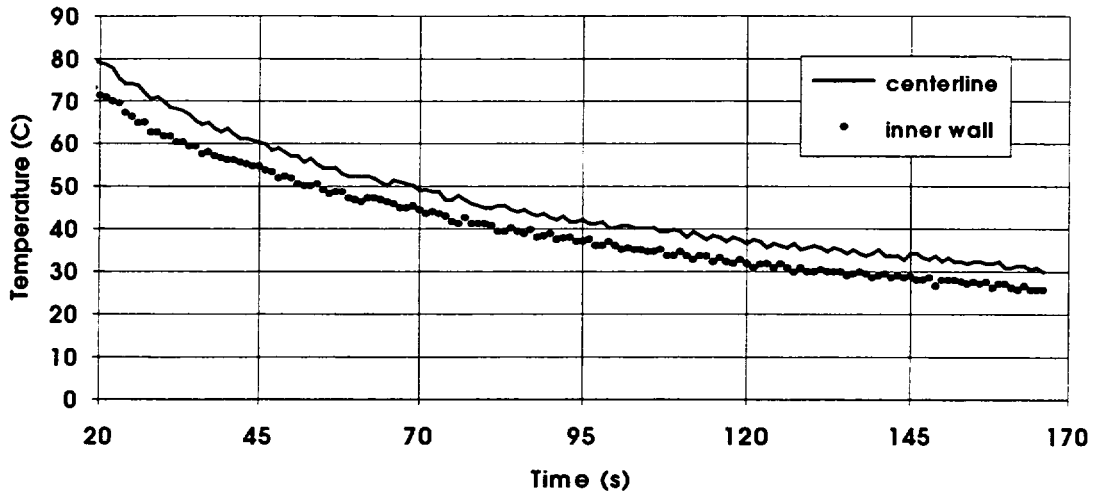


Figure 3.2. Comparison of Centerline and Inner Wall Temperatures  
(Position of Thermocouples: 0.958 m from top)

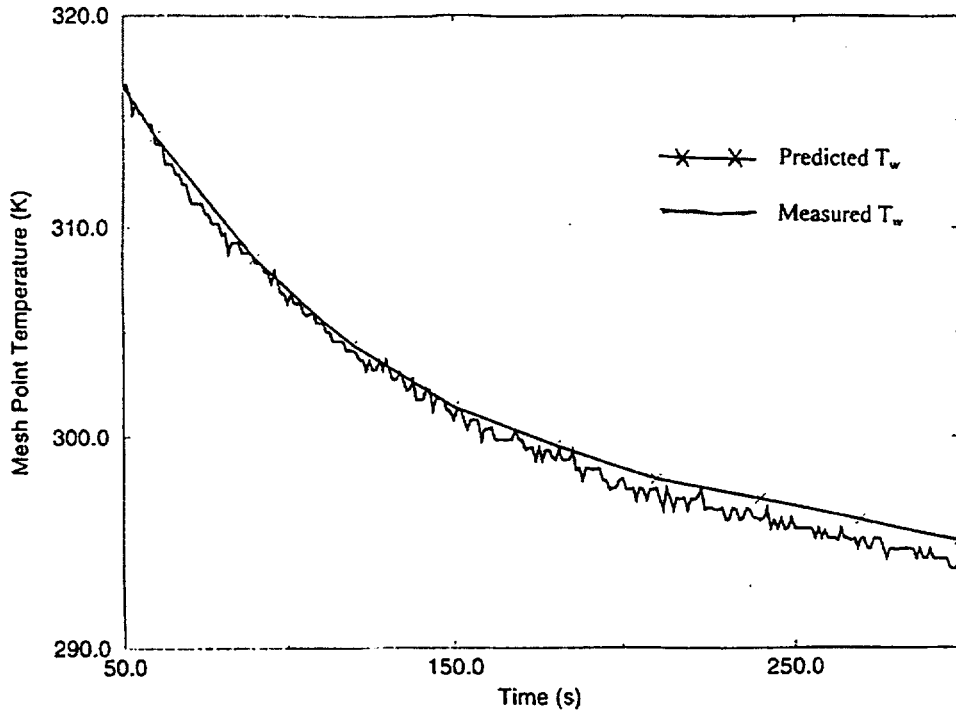


Figure 3.3. Comparison of Predicted (RELAP5) and Measured  
Inner Wall Temperature

### 3.1.4 Reproducibility of Data

It is important to demonstrate the reproducibility of the data and some experiments were repeated at nearly the same operating conditions to see whether the data can be reproduced reasonably close. The results of two sets of experiments are presented in Figures 3.4 and 3.5, for the nominal system pressures of 2 and 3 bars. The experimental boundary conditions are given in Chapter 4. The inlet air mass fraction of these experiments is about 10%. Maximum deviation found from these two sets of experiments are; 6% and 10%, for  $P_n=2$  bars and  $P_n=3$  bars, respectively. Primary reasons of deviation are the system pressure, vapor flow rate, and cooling water flow rate. However, the percent deviations may be considered as reasonable when the uncertainty band of heat flux is considered. The uncertainty band of heat flux was calculated to be 11% (Appendix B).

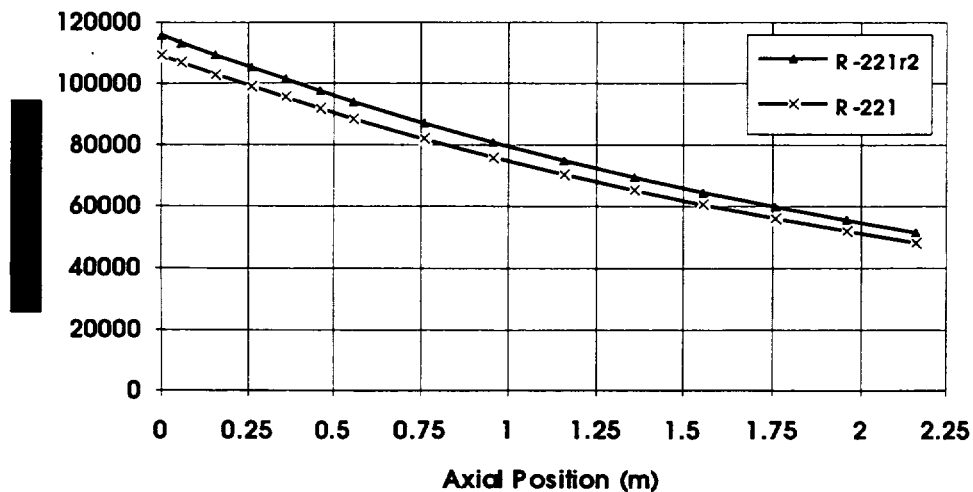


Figure 3.4. Test of Reproducibility of Experimental Data  
( $P_n=2$  bars,  $X_i=10\%$ )

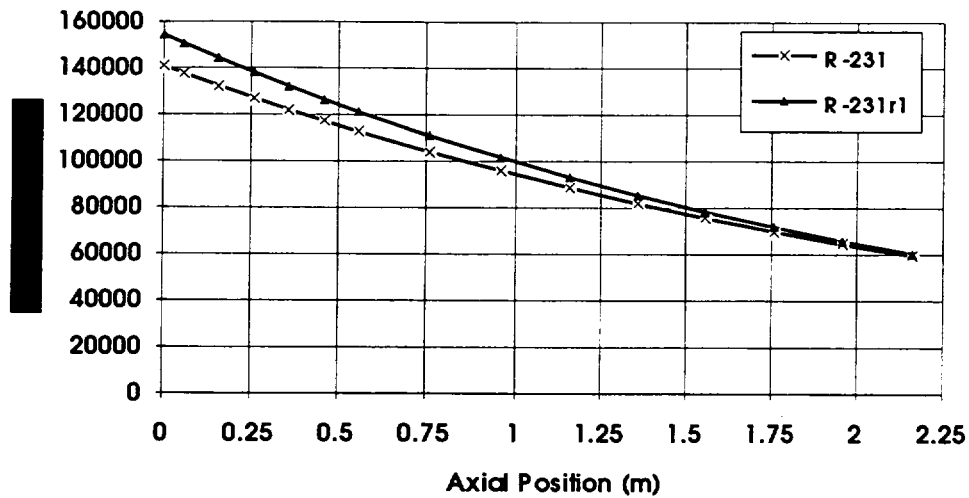


Figure 3.5. Test of Reproducibility of Experimental Data  
 $(P_n=3 \text{ bars}, X_i=10 \%)$

### 3.2 Experiments

The experimental procedure comprises the stages of system start-up, transient process to steady-state condition, data logging, and system shutdown.

#### 3.2.1 System Start-up

First step for the system start-up is the preparation of the boiler by checking water inventory. Then system check is made through the control of the following equipment:

1. Valve position of fresh water inlet of the boiler: closed
2. Valve position of compressed air inlet to the boiler: closed
3. Isolation valve of the boiler: closed
4. Control of boiler pressure controller: set to the predetermined pressure level
5. Control of electrical heaters
6. Drainage of condensate accumulated inside of the rotameters at the exit of the compressor tanks

7. Control of pressure inside of compressor tanks
8. Start of cooling water flow through the jacket pipe
9. Adjust the flow rate to a predetermined value
10. Open the valve at the exit of the discharge tank
11. Open the boiler isolation valve slowly when pressurization is completed
12. Dump vapor to atmosphere for at least 15 minutes
13. Check for temperature reading at upstream of the test section whether air was swept out by vapor flow.
14. Adjust system pressure and vapor flow rate by controlling the valve at the exit of the discharge tank
15. Turn on the electrical pre-heaters
16. Open valve for air injection
17. Adjust air flow rate via rotameter

### **3.2.2 Operating at Steady-state Conditions and Data Logging**

The control of the steady-state conditions was performed by monitoring the system parameters, i.e. temperature, pressure, and flow rate, on computer via data acquisition system. Data recording was not started before desired steady-state operating condition was reached. After steady-state condition was sustained, the data logging was started. Data were recorded with one second intervals approximately for a two minutes period. During data logging, special care was given to the control of compressed air flow rate, vapor or mixture flow rate, and system pressure.

### **3.2.3 System Shutdown**

System shutdown was started by putting off the electrical heaters in the boiler and at the pre-heating section. Then, compressed air injection was terminated along with fully opening of the valve at the exit of the discharge tank. Vapor inside the dome of the boiler was discharged till the system pressure was about 1 bar. Finally, the cooling water flow was terminated.

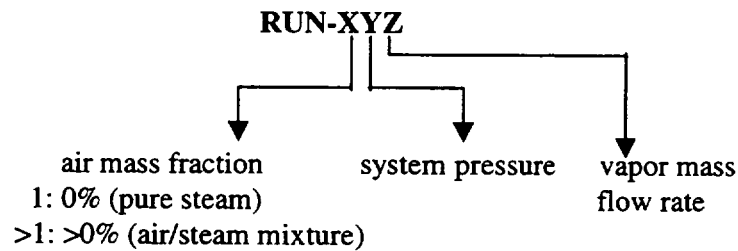
## CHAPTER 4

### EXPERIMENTAL TEST MATRIX

The experimental test matrix consists of two parts: pure steam runs and air/steam mixture runs. The following parameters were considered while generating this matrix:

- 1- system pressure,
- 2- steam flow rate,
- 3- air mass fraction.

The experimental test matrices are given in Table 6.1 and Table 6.2. The coding of these experimental runs are based on the following logic:



It is to be noted that the mass flow rate measurement was performed by using a differential pressure transmitter (orifice meter) so that in each set of experimental run, differential pressure, rather than mass flow rate, was set to an almost constant predetermined value while changing system pressure. This means, that the vapor mass flow rate increases as the system pressure increases ( $Z=1$ ). In air/steam mixture runs, system pressure and steam mass flow rate settings are kept close to those set before during pure steam runs. The reason of selecting steam mass flow rate as a fixed parameter, rather than total mixture mass flow rate, in air/steam mixture runs is to fix the amount of steam at the entrance of the test section to be able to make better comparison with the data of pure steam runs and to understand inhibiting effect of air as a noncondensable gas. However, the total mass flow rate (mass flow rate of air + vapor) was increased compared to the pure steam runs and this should be taken into account

when analyzing the experimental data. Some additional experimental runs ( $Z=2$ ) were performed by using same vapor flow rate and different system pressure: RUN-1.2.2 and RUN-1.3.2 based on vapor flow rate of RUN-1.4.1, RUN-3.3.2 based on vapor flow rate of RUN-3.4.1R1 and RUN-5.3.2 based on vapor flow rate of RUN-5.4.1. Besides these, the total mass flow rate (vapor+air) was kept same ( $Z=3$ ) as the mass flow rate of corresponding pure steam run(s) while keeping the system pressure same but varying the air quality only: RUN-3.4.3 and RUN-5.4.3 based on the vapor mass flow rate of RUN-1.4.1, RUN-3.2.3 based on the vapor mass flow rate of RUN-1.2.1 and RUN-3.3.3 based on the vapor mass flow rate of RUN-1.3.1.

The effect of inlet superheating was checked by the runs with the extension of 'NH' which stands for 'No Heating' at the inlet of the condenser tube. It is to be noted that other runs without the extension of 'NH' were performed with certain steam superheating degree at the inlet of the condenser tube. The extension 'R' means repeated run with the same inlet conditions. However, in some cases, the base runs of repeated ones are not given since those runs are not that reliable.

Table 4.1 Test Matrix for Pure Steam Experimental Runs

Code	P (bars)	$\dot{m}_v$ (kg/s)	$Re_v$	$\dot{m}_{cw}$ (kg/s)	$X_{air}$
RUN-1.1.1	1.376	$1.409 \times 10^{-2}$	43814	0.177	0.0
RUN-1.2.1	1.829	$1.808 \times 10^{-2}$	54770	0.221	0.0
RUN-1.2.1R	1.799	$1.812 \times 10^{-2}$	54991	0.242	0.0
RUN-1.3.1	3.029	$2.314 \times 10^{-2}$	66875	0.223	0.0
RUN-1.4.1	3.959	$2.721 \times 10^{-2}$	76645	0.226	0.0
RUN-1.5.1	4.837	$3.101 \times 10^{-2}$	85675	0.225	0.0
RUN-1.6.1	5.452	$3.419 \times 10^{-2}$	93365	0.226	0.0
RUN-1.2.1NH	1.919	$1.831 \times 10^{-2}$	55236	0.233	0.0
RUN-1.3.1NH	2.970	$2.297 \times 10^{-2}$	66502	0.237	0.0
RUN-1.4.1NH	3.91	$2.701 \times 10^{-2}$	76187	0.239	0.0
RUN-1.2.2	1.919	$2.740 \times 10^{-2}$	77183	0.240	0.0
RUN-1.3.2	3.1	$2.800 \times 10^{-2}$	80742	0.240	0.0

Table 4.2 Test Matrix for Air/Steam Experimental Runs

Code	P (bars)	$\dot{m}_v$ (kg/s)	$Re_v$	$\dot{m}_{cw}$ (kg/s)	$X_{air}$
RUN-2.1.1	1.544	$1.465 \times 10^{-2}$	45091	0.199	0.106
RUN-3.1.1R	1.454	$1.530 \times 10^{-2}$	47957	0.229	0.194
RUN-4.1.1R	1.469	$1.776 \times 10^{-2}$	55694	0.232	0.211
RUN-2.2.1	1.919	$1.771 \times 10^{-2}$	53748	0.198	0.099
RUN-2.2.1R2	1.919	$1.853 \times 10^{-2}$	56228	0.232	0.095
RUN-3.2.1	1.956	$1.865 \times 10^{-2}$	56879	0.236	0.191
RUN-4.2.1	2.01	$2.055 \times 10^{-2}$	62949	0.232	0.275
RUN-2.3.1	2.969	$2.306 \times 10^{-2}$	66771	0.23	0.099
RUN-2.3.1R1	2.93	$2.428 \times 10^{-2}$	70801	0.232	0.092
RUN-3.3.1	2.901	$2.366 \times 10^{-2}$	69543	0.231	0.189
RUN-4.3.1	3.16	$2.664 \times 10^{-2}$	78258	0.238	0.279
RUN-5.3.1R	3.13	$1.804 \times 10^{-2}$	53938	0.237	0.421
RUN-2.4.1	3.982	$2.833 \times 10^{-2}$	80253	0.234	0.097
RUN-3.4.1	3.90	$2.77 \times 10^{-2}$	79188	0.223	0.193
RUN-3.4.1R1	3.79	$2.644 \times 10^{-2}$	75884	0.237	0.208
RUN-4.4.1	3.94	$2.987 \times 10^{-2}$	85898	0.231	0.274
RUN-5.4.1	3.94	$2.193 \times 10^{-2}$	63663	0.253	0.369
RUN-6.4.1	3.906	$1.526 \times 10^{-2}$	45195	0.253	0.519
RUN-2.5.1	4.312	$2.918 \times 10^{-2}$	82043	0.237	0.097
RUN-6.5.1	4.36	$1.881 \times 10^{-2}$	54476	0.253	0.43
RUN-2.6.1	5.257	$3.386 \times 10^{-2}$	93388	0.234	0.098
RUN-2.2.1NH	1.88	$1.748 \times 10^{-2}$	53269	0.237	0.130
RUN-2.3.1NH	2.93	$2.416 \times 10^{-2}$	70480	0.237	0.098
RUN-2.4.1NH	4.06	$2.864 \times 10^{-2}$	81074	0.237	0.113
RUN-3.4.1NH	3.79	$2.630 \times 10^{-2}$	75697	0.237	0.242
RUN-4.4.1NH	3.87	$2.982 \times 10^{-2}$	85980	0.237	0.284
RUN-5.4.1NH	4.09	$2.109 \times 10^{-2}$	61278	0.240	0.408
RUN-3.3.2	2.97	$2.749 \times 10^{-2}$	80492	0.240	0.168
RUN-5.3.2	2.97	$2.380 \times 10^{-2}$	70533	0.241	0.310
RUN-3.4.3	3.98	$2.118 \times 10^{-2}$	60615	0.241	0.230
RUN-5.4.3	3.94	$1.647 \times 10^{-2}$	47968	0.241	0.398
RUN-3.2.3	1.90	$1.276 \times 10^{-2}$	39293	0.250	0.276
RUN-3.3.3	3.27	$1.900 \times 10^{-2}$	55369	0.250	0.223

## CHAPTER 5

### DATA REDUCTION PROCEDURE

The following steps were used for data reduction:

- A. Averages of all the measured parameters were taken for 10 s and recorded on the computer during experiments. The total data logging period of experiments were about 1.5–2 minutes. The oscillatory behavior was observed only for cooling water temperature with a period of 3–4 s, however, the amplitude of the oscillations was small ( $\pm 1$  °C). The source of such oscillations observed for the jacket cooling water measurements was turbulence inside the annular region of the jacket pipe, as expected.
- B. The following exponential curve was used to fit the cooling water temperature data measured inside the jacket pipe,

$$T(x) = Ae^{-Bx} \quad (5.1)$$

Before a decision was given for the type of fitting, different forms were tested, such as polynomials, power law, quadratic, and exponential. In general, all these types of fitting models yield close results with respect to the correlation coefficient which is defined as

$$r = \sqrt{\frac{\sigma^2 - S^2}{\sigma^2}} \quad (5.2)$$

where  $\sigma$  and  $S$  are standard deviation and deviation from the fitting curve. However, exponential form is more realistic when the behavior of the heat flux, as the function of the axial distance, is concerned. The correlation coefficient was calculated to be between 0.98 and 1.0, which is quite acceptable.

C. Spatial derivative of cooling water temperature  $T(x)$  found in step (B) was used to predict the heat flux profile in the annulus of jacket pipe. Since the environmental heat loss from the jacket pipe is very low no correction was applied to the heat flux profile prediction. The local heat flux at the inner tube wall, based on inner diameter ( $d_i$ ) of the condenser tube, was calculated from

$$q''(x) = -\frac{\dot{m}_{cw} c_p}{\pi d_i} \frac{dT_{cw}(x)}{dx} \quad (5.3)$$

The derivation of Equation (7.3) was based on the energy balance given in Figure 5.1, for steady state and steady flow conditions.

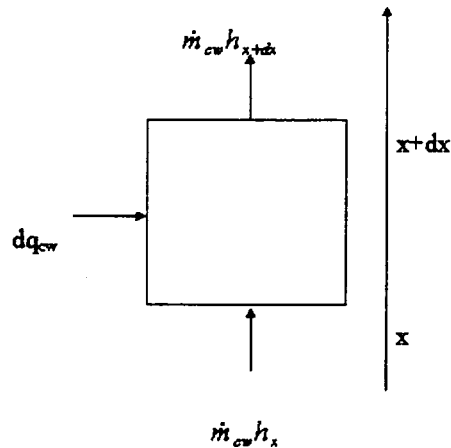


Figure 5.1. Energy Balance on a Control Volume of the Jacket Pipe

The energy balance then yields

$$dq_{cw} = \dot{m}_{cw} (h_{x+dx} - h_x) \quad (5.4)$$

or

$$dq_{cw} = \dot{m}_{cw} dh \quad (5.5)$$

and by inserting  $dh=c_p dT$ , we get

$$dq_{cw} = \dot{m} c_p dT \quad (5.6)$$

D. The experimental heat transfer coefficient was then calculated from

$$h(x) = \frac{q''(x)}{T_c(x) - T_w(x)} \quad (5.7)$$

E. The absolute system pressure was calculated from the measured gauge pressure at the inlet of the test section by considering the measured local absolute pressure in Ankara. This modification for the measured absolute system pressure was needed to calculate the correct saturation temperature of vapor at the inlet of the test section, and partial pressure and saturation temperature of vapor along the tube.

F. The mass flow rate of vapor or air/vapor mixture and associated Reynolds number were calculated. For this step, the calibration data of the orifice, i.e. flow coefficient and Reynolds number relation given in Section 2.4.3, were used.

Mass flow rate computation is purely a mathematical process once a calibration curve of the orifice has been generated. Since flow coefficient is dependent on Reynolds number, which is itself dependent on mass flow rate, final value of the flow coefficient, and hence of mass flow rate, can be obtained iteratively using an initial chosen value of Reynolds number.

For the computation of mass flow rate, the method given in BSI-1042 [5] was used. Initial guess for the Reynolds number was  $10^6$  and the iterative procedure included the calculation

of flow coefficient from Equation 2.1, and mass flow rate from the relation of Reynolds number based on internal pipe diameter (D) at the upstream of the orifice:

$$\text{Re}_D = \frac{\dot{m}D}{A_D\mu} \quad (5.8)$$

Here  $\dot{m}$  and  $\mu$  are given for vapor or air/vapor mixture, depending on the method of air injection, i.e. if air is injected to water inside the boiler then mixture properties should be used.

Then, differential pressure over the orifice as calculated from

$$\Delta P = \frac{1}{2\rho} \left( \frac{\dot{m}}{\alpha \frac{\pi}{4} d^2} \right)^2 \quad (5.9)$$

was compared to the one measured and the iteration, by changing the Reynolds number guess, continued till the calculated differential pressure was equal to the measured one. The density ( $\rho$ ) in Equation (5.9) is calculated by considering upstream condition of the orifice (vapor or air/vapor mixture depending on the method of air injection).

## CHAPTER 6

### EXPERIMENTAL RESULTS AND DISCUSSION

#### 6.1 Introduction

Some of the selected experimental results are presented in this chapter [2,9]. The whole range of the data was included into the USNRC Data Bank. The parameters considered are; centerline, inner wall and cooling water temperature distributions, heat flux profile, and predicted local air mass fraction and film Reynolds number distributions along the flow direction.

#### 6.2 Temperature Distribution

Temperature measurements were performed at three different locations in the radial direction of the test section: at the centerline and inner wall of the condenser tube, and at the annulus of the jacket pipe. The centerline temperature simply gives the information for the state of vapor, flowing downward, along with the system pressure measured at the inlet of the test section. It is expected that for pure steam runs, the measured centerline temperature should be the saturation temperature at the corresponding system pressure measured at the inlet, by assuming that differential pressure along the channel is small enough ( $\sim 0.3$  bar at the system pressure of 5 bars, and much smaller for lower system pressure settings). Moreover, when air/vapor mixture flows along the test section, the centerline temperatures indicate the existence of air at the core of the condenser tube since the vapor temperature is lower than the saturation temperature corresponding to the total system pressure due to partial pressure of vapor phase which decreases with increasing quality of air, as Gibbs-Dalton Law states. Measured inner wall temperature values also indicate the effect of the presence of air as a noncondensable gas, by following the trend of centerline temperature, i.e. higher the percentage of air lower the centerline and inner wall temperatures. In fact, air, presumably homogeneously mixed with vapor at the entrance of the test section, then tends to accumulate at the interface of liquid film and air/vapor mixture which, consequently, causes a corresponding reduction of partial pressure of vapor at the interface. In turn, this reduces the

saturation temperature at which condensation takes place. The net effect is to lower the effective thermal driving force ( $T_i - T_w$ ) thereby reducing the heat transfer rate. The accumulation of air at the interface is the principal reason for the mass diffusion resistance in radial direction which causes lower condensation rates. The mechanism of air accumulation at the interface of air/vapor and liquid film can be explained on the following physical grounds: The vapor that is to be condensed is carried towards the wall of the condenser tube and it also carries with it some amount of air. Since the condensate film is impermeable to air, it must be removed from the interface at the same rate as it arrives, at steady-state conditions. However, the rate of diffusive flow depends on the concentration gradient and sufficient amount of gas should be accumulated at the interface to sustain the balance between the convective inflow and diffusive back-flow.

The temperature measurement in the jacket pipe, on the other hand, enables the prediction of the local heat flux distribution inside the condenser tube as described in Chapter 5.

The measured temperature distributions of the experimental runs corresponding to the nominal system pressure of 2 bars are presented in Figures 6.1–6.3.

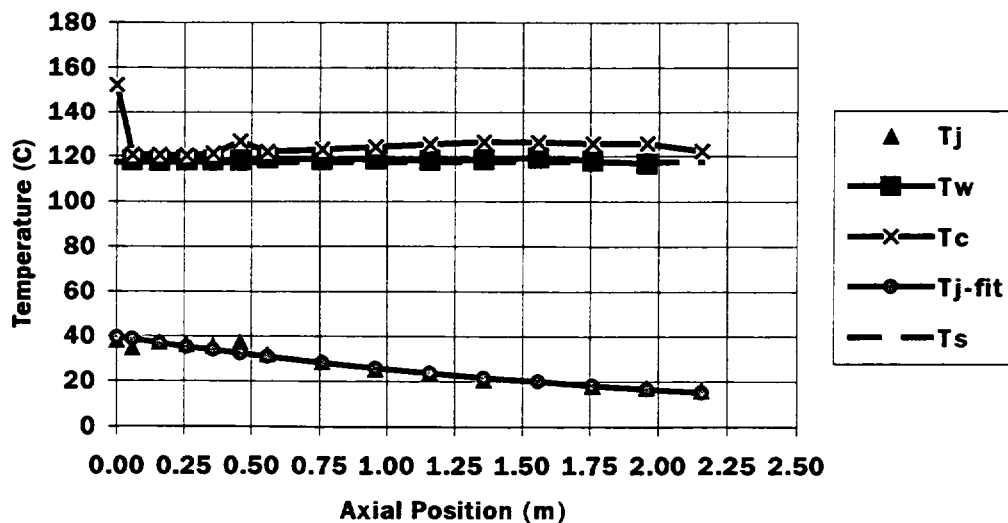


Figure 6.1. Temperature Distribution ( $P_n=2$  bars,  $Re_v=54770$ ,  $X_i=0\%$ )

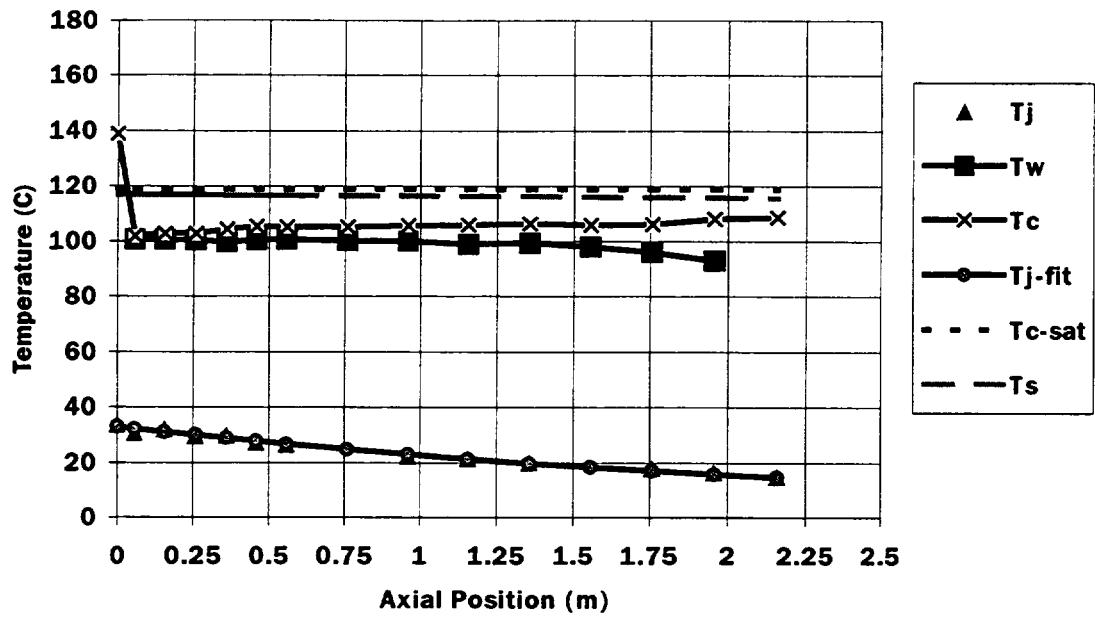


Figure 6.2. Temperature Distribution ( $P_n=2$  bars,  $Re_v=56228$ ,  $X_i=10\%$ )

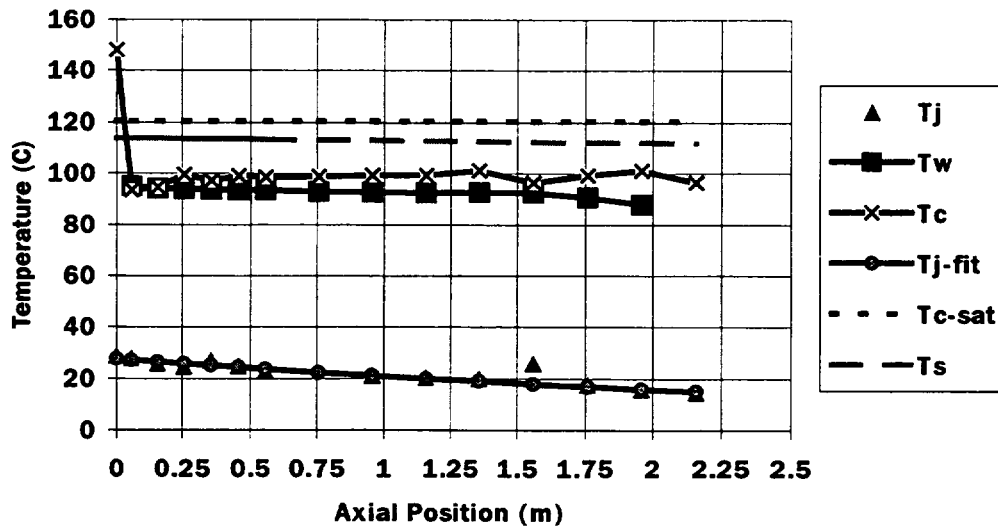


Figure 6.3. Temperature Distribution ( $P_n=2$  bars,  $Re_v=62949$ ,  $X_i=28\%$ )

These three experiments were performed at nearly the same operating condition concerning the system pressure and inlet superheating degree of vapor. When results given in Figures 6.2 and 6.3 are compared to those given in Figure 6.1 (pure vapor), following results can be drawn at first glance: centerline and condenser tube inner wall temperature distributions are almost constant throughout the tube length regardless of the inlet air quality. The centerline, wall and cooling water temperatures decrease as inlet air quality increases. As can be seen in Figure 6.1, the centerline and wall temperatures are very close to the saturation temperature (around 120 °C), corresponding to the system pressure, especially at the entrance of test section. It is to be noted that the rate of condensation, along with the cooling water and vapor mass flow rates, becomes important regarding the rate of detachment of the liquid droplets from the condensed liquid film over the tube surface towards the thermocouples which are attached to a guide wire at the centerline of the tube. That is to say, when the rate of condensation increases the measured centerline temperatures tend to decrease (centerline temperature subcooling effect) due to higher rate of detachment of liquid droplets or patches from the surface. In the test matrix under consideration, the aforementioned effect is more pronounced as system pressure and vapor flow rate are increased, i.e. the former is effective for higher heat flux whereas the later is responsible for agitating turbulence of liquid film on the inner surface of the condenser tube. If, somehow, the operating condition reverses then the inlet superheating of the vapor becomes more sensible, as seen in Figure 6.1.

In Figures 6.2 and 6.3, it is observed that, difference between the saturation temperature ( $T_{c-sat}$ ), corresponding to the system pressure measured at the inlet of the test section, and the measured centerline temperature ( $T_c$ ) increases as the inlet air quality increases, i.e. on the average,  $\Delta T=11-17$  °C and  $19-27$  °C, for  $X_i=10$  % and  $28$  %, respectively. In reality, the saturation temperature also decreases as the local mass fraction of air increases and this is shown in Figures 6.2 and 6.3 by the parameter ' $T_s$ '.  $T_s$  was calculated from the predicted local vapor pressure given by the Gibbs-Dalton ideal gas mixture equation:

$$P_s = \frac{P_t(X_{air} - 1)}{\left[ \left( 1 - \frac{M_v}{M_{air}} \right) X_{air} - 1 \right]} \quad (6.1)$$

where the local air mass fraction ( $X_{\text{air}}$ ) was predicted from the sectionwise energy balance.

Difference between the saturation temperature of pure vapor ( $T_{\text{c-sat}}$ ) and predicted saturation temperature of air/vapor mixture ( $T_s$ ) is about 3 °C for the case with  $X_i=10\%$ , and 7 °C for the case with  $X_i=28\%$ . The marked increase of the temperature difference ( $T_{\text{c-sat}}-T_s$ ) in two cases as presented in Figures 6.2 and 6.3 is the result of increase of the inlet air mass fraction, as expected. Another point worth to mention is that an inequality between  $T_c$  and  $T_s$  ( $T_c < T_s$ ) is observed for all cases, except the pure vapor case, and the difference of  $T_s$  and  $T_c$  increases from 9–14 °C to 13–19 °C by an increase of air mass fraction from 10 % to 28 %. This can be attributed to the lowered inner wall temperature due to higher air mass fraction, which in turn lowers the measured centerline temperature as well. This situation indicates that the measured centerline temperature was highly affected by the prevailing inner wall thermal conditions, probably, due to detached liquid droplets which lowers the measured centerline temperature ( $T_c$ ). This is important since this situation, i.e. having inequality between measured and predicted centerline temperatures ( $T_c < T_s$ ), leads to the conclusion that pattern of the core flow inside the condenser tube is likely to be homogeneous two-phase flow mixed with air. It should be noted that two-phase flow condition inside the tube makes it difficult to predict the condensation heat transfer coefficient since selecting either of centerline temperatures, that is the measured or the predicted one, for calculating the heat transfer coefficient may lead to considerably different local values.

The measured temperature distributions of the experimental runs corresponding to the nominal system pressure of 4 bars are presented in Figures 6.4–6.7. All of the temperatures are elevated compared to the previously discussed case due to higher system pressure and inlet temperature. It should be noted that experimental runs with the system pressure of 4 bars were performed at the condition of higher vapor Reynolds number compared to the case with 2 bars, i.e. the vapor Reynolds number is about 50 % higher than the case with 2 bars system pressure.

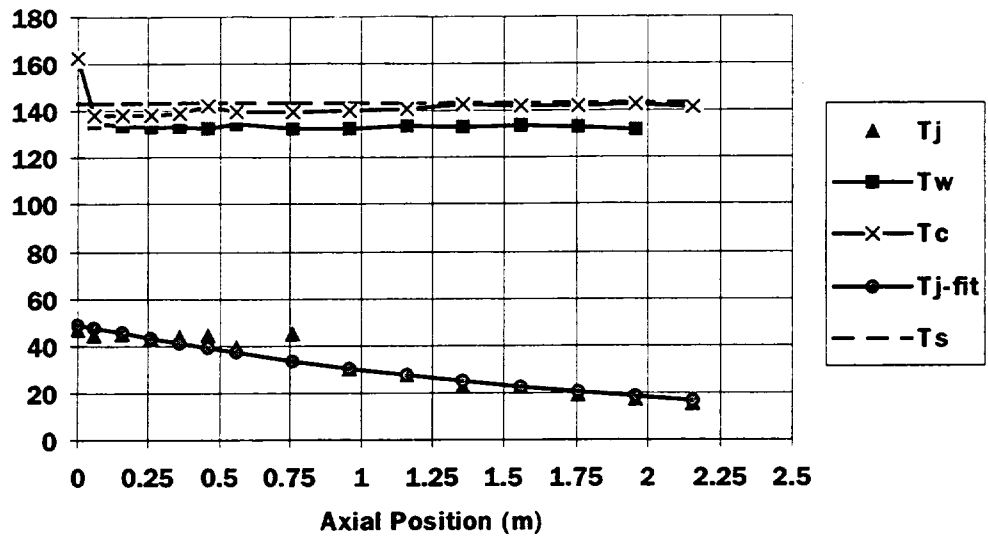


Figure 6.4. Temperature Distribution ( $P_n=4$  bars,  $Re_v=76645$ ,  $X_i=0$  %)

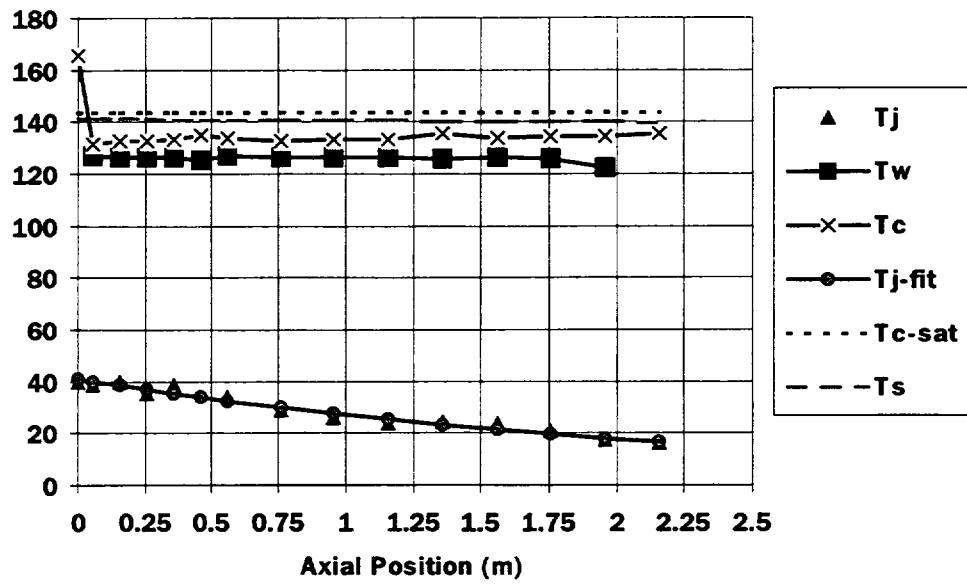


Figure 6.5. Temperature Distribution ( $P_n=4$  bars,  $Re_v=80253$ ,  $X_i=10$  %)

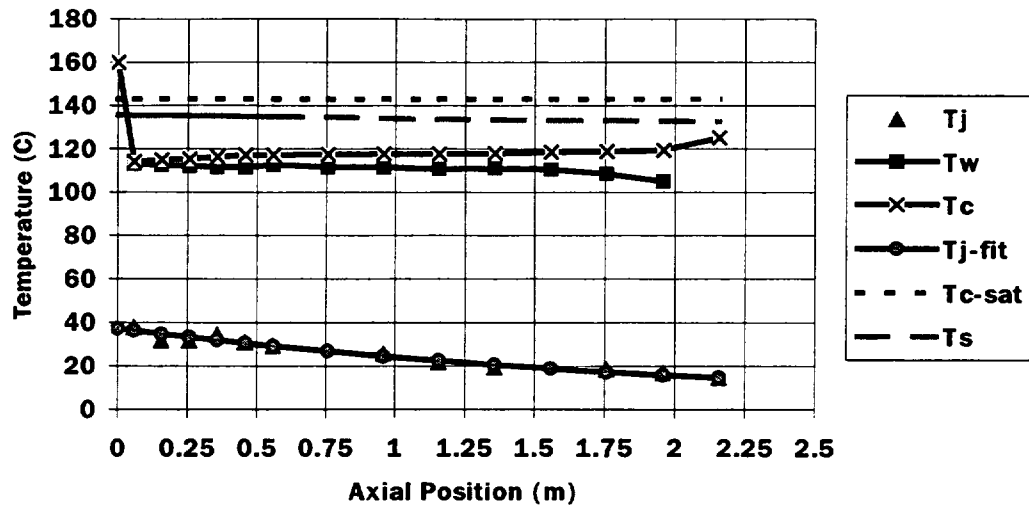


Figure 6.6. Temperature Distribution ( $P_n=4$  bars,  $Re_v=85898$ ,  $X_i=28$  %)

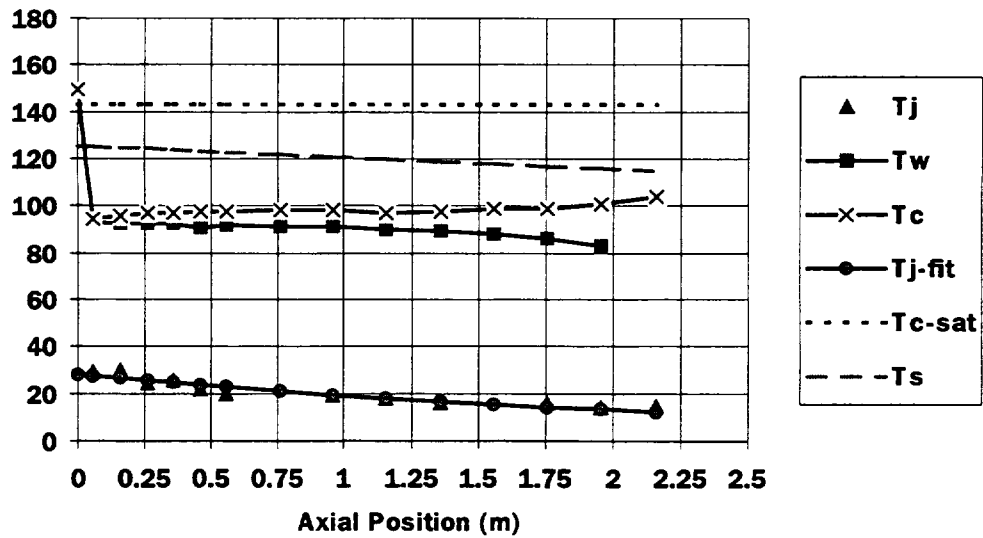


Figure 6.7. Temperature Distribution ( $P_n=4$  bars,  $Re_v=45195$ ,  $X_i=52$  %)

The pure vapor run results show that the measured centerline temperature ( $T_c$ ) trend closely follows the saturation temperature ( $T_s$ ) line and always remains below of it, with a maximum difference of about 4 °C, even at the bottom of the test section. It is observed from the comparison of pure vapor runs with the nominal system pressure of 2 bars and 4 bars, that the absolute temperature difference ( $T_s - T_c$ ) decreases by increase of  $Re_v$ , and the effect of inlet superheating is no longer observable for the case with the pressure of 4 bars. This may be the result of subcooling at the centerline of the condenser tube due to increased rate of detachment of liquid droplets from condensate film. The temperature differences of  $T_{c-sat}$  (saturation temperature of zero air quality) and  $T_c$  are: 9–12 °C, 24–29 °C and 42–48 °C for the cases of  $X_i = 10\%$ , 28% and 52%, respectively. The differences between the predicted (from the Gibbs-Dalton Law,  $T_s$ ) and the measured ( $T_c$ ) centerline temperatures come out to be 1–5 °C, 5–9 °C, 13–21 °C, and 15–31 °C, for  $X_i = 0\%$ , 10%, 28%, and 52%, respectively. The temperature difference ( $T_{c-sat} - T_c$ ) can be attributed to the existence of air and cooling of centerline thermocouples by liquid droplets. Among the results presented, the experimental results pertaining to the case with  $X_i = 52\%$  represents a special case concerning the inlet vapor Reynolds number (~41000), which is about half of other runs at the same pressure setting. The distribution of  $T_s$  shows a marked decrease towards the bottom of tube due to increase in  $X$ , steeper than other runs. Moreover, a sharp decrease in all measured temperatures ( $T_c$ ,  $T_w$ ) are observed for the case with  $X_i = 52\%$ , i.e. about 40 °C, relative to the pure vapor case.

### 6.3 Local Heat Flux Distribution

To calculate local heat transfer coefficients, the local air/vapor mixture temperature, local inner wall temperature, and the local heat flux must be known. The local air/vapor mixture and inner wall temperatures were measured directly, and the local heat flux was obtained from the measured coolant temperature profile. Hence, the local axial temperature gradient ( $dT_{cw}/dx$ ) was computed from an exponential fit of the measured coolant temperature as a function of axial distance and the local heat flux was determined from:

$$q''(x) = -\frac{\dot{m}_{cw} c_p}{\pi d_i} \frac{dT_{cw}(x)}{dx} \quad (6.2)$$

The heat flux distributions for experimental runs corresponding to the nominal system pressures of 2–6 bars, and including pure vapor and different mixtures of air and vapor, are presented in Figs. 6.8–6.12 (X in these figures stands for inlet air mass fraction).

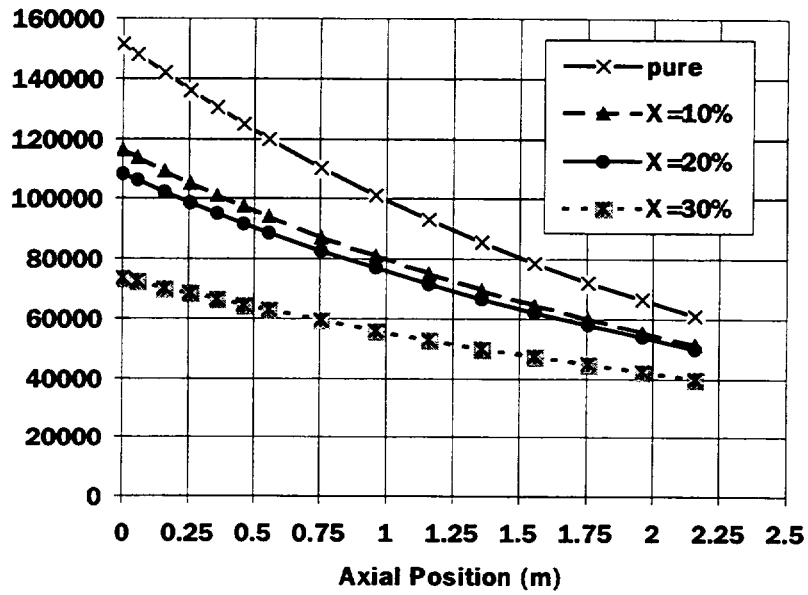


Figure 6.8. Heat Flux Distribution along the Condenser Tube  
( $P_n=2$  bar,  $Re_v=54000-63000$ )

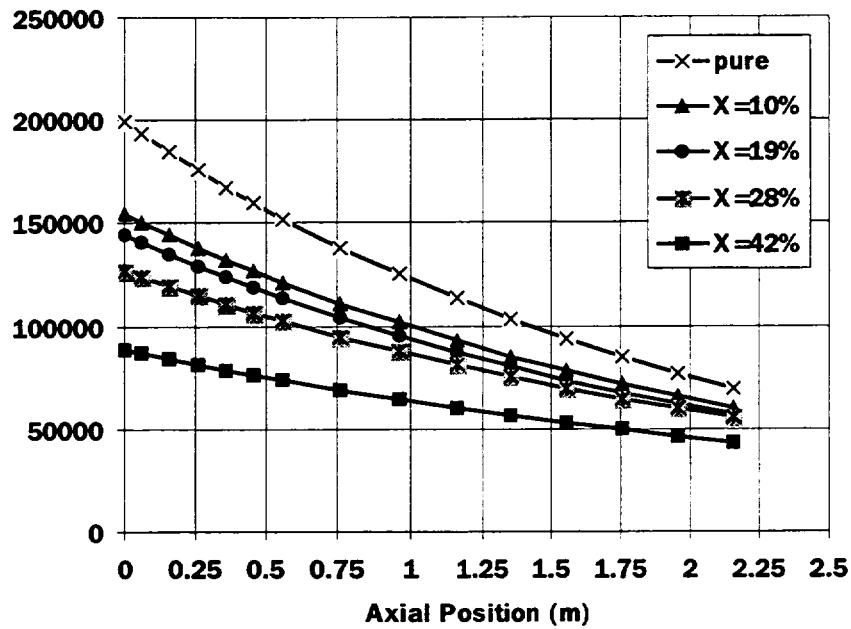


Figure 6.9. Heat Flux Distribution along the Condenser Tube  
 ( $P_n=3$  bars,  $Re_v=67000-78000$  and  $Re_v=54000$  for  $X_i=42\%$ )

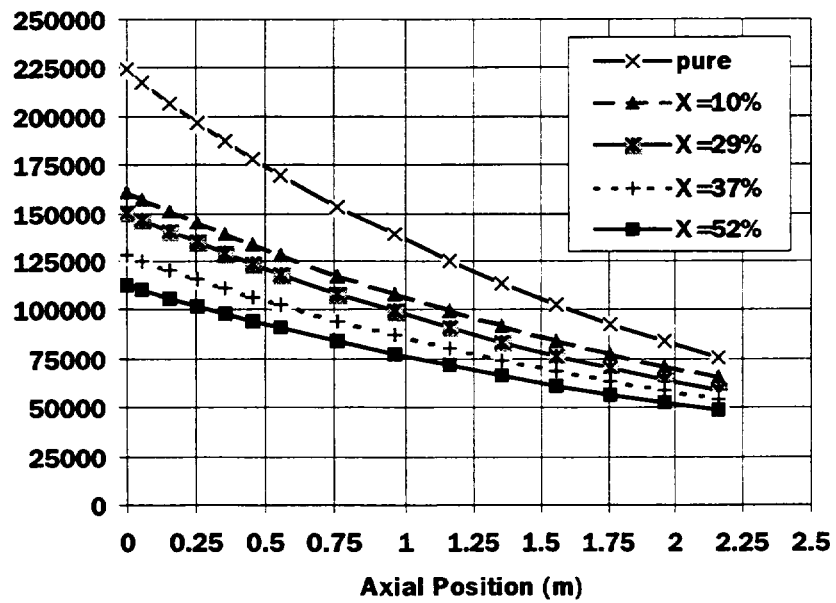


Figure 6.10. Heat Flux Distribution along the Condenser Tube  
 ( $P_n=4$  bar,  $Re_v=77000-86000$  and  $Re_v=45000$  for  $X_i=52\%$ )

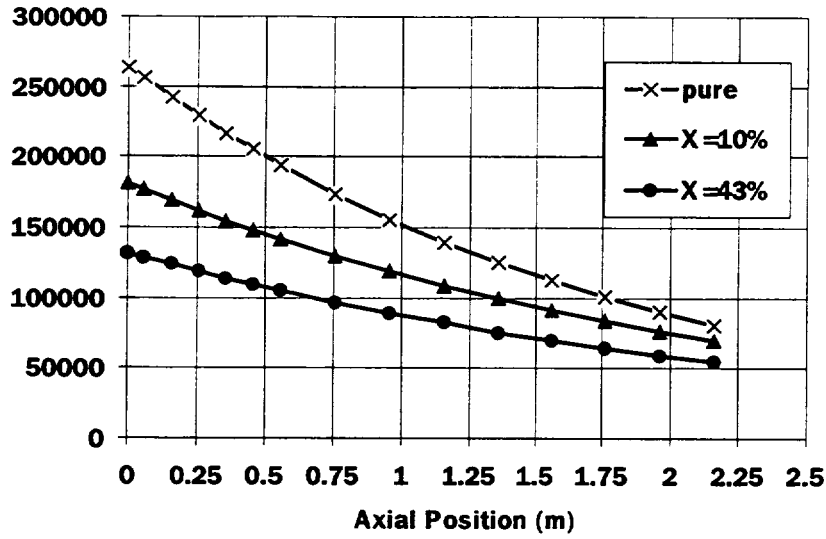


Figure 6.11. Heat Flux Distribution along the Condenser Tube  
 ( $P_n=5$  bar,  $Re_v=82000-86000$  and  $Re_v=55000$  for  $X_i=43\%$ )

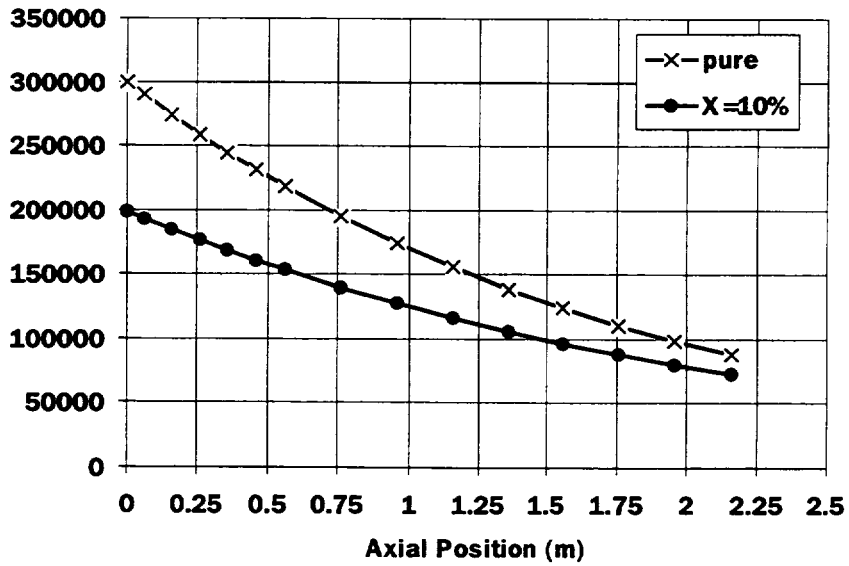


Figure 6.12. Heat Flux Distribution along the Condenser Tube  
 ( $P_n=6$  bars,  $Re_v=93000$ )

It is clear in these figures that the heat flux drastically decreases as inlet air mass fraction increases. This situation is the evidence for how some amount of air, mixed with vapor, degrades the performance of the heat exchanger. By referring to Figures 6.8–6.12, decrease in local heat flux at the middle of the test section ( $\sim 1$  m from the top) as compared to the corresponding pure vapor case is summarized as:

- $P_n=2$  bar: 20 % ( $X_i=10$  %), 24 % ( $X_i=20$  %), 45 % ( $X_i=30$  %)
- $P_n=3$  bar: 19 % ( $X_i=10$  %), 24 % ( $X_i=19$  %), 30 % ( $X_i=28$  %), 48 % ( $X_i=42$  %)
- $P_n=4$  bar: 22 % ( $X_i=10$  %), 24 % ( $X_i=20$  %), 28 % ( $X_i=29$  %), 37 % ( $X_i=37$  %)  
44 % ( $X_i=52$  %)
- $P_n=5$  bar: 24 % ( $X_i=10$  %), 75 % ( $X_i=43$  %)
- $P_n=6$  bar: 27 % ( $X_i=10$  %)

Another point to be emphasized is that local heat flux values for pure steam and air/steam mixture runs get closer towards the bottom of the condenser tube due to diminishing condensation rate as the result of increased resistance of condensate film. This means that condensate film resistance in pure steam runs tends to dominate over diffusion resistance in air/steam mixture runs, at the bottom of the condenser tube.

An increase in system pressure increases local heat flux and this can be attributed to the increase in wall subcooling degree that enhances the thermal driving force for heat transfer. Moreover, higher system pressure associated with the higher inlet temperature leads to a greater number of molecular collisions helping in the diffusive transport of energy. However, in our experimental investigation, the dependency of the wall subcooling degree, either measured ( $T_c - T_w$ ) or predicted from Gibbs-Dalton Law ( $T_s - T_w$ ), on system pressure is such that the wall subcooling degree remains nearly the same for the same inlet air mass fraction and for the different system pressure. This implies that the vapor mass flow rate may dominate over system pressure, concerning the effect on local heat flux, for cases with air/vapor mixture (Figure 6.14). The situation is rather different in pure vapor runs, that is increase in system pressure has a strong effect on enhancement of predicted, and even measured, wall subcooling degree and hence on increase of local heat flux (Figure 6.13).

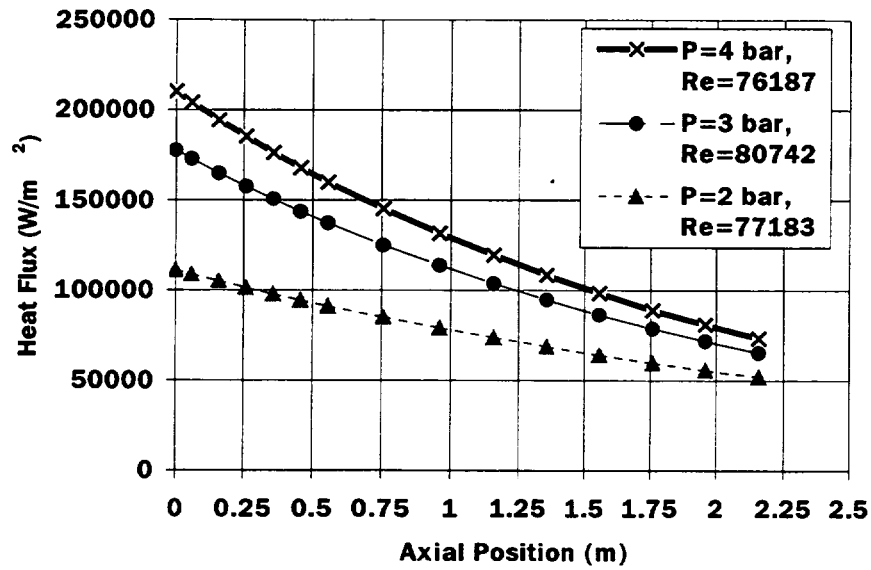


Figure 6.13. Effect of System Pressure (Pure Steam)

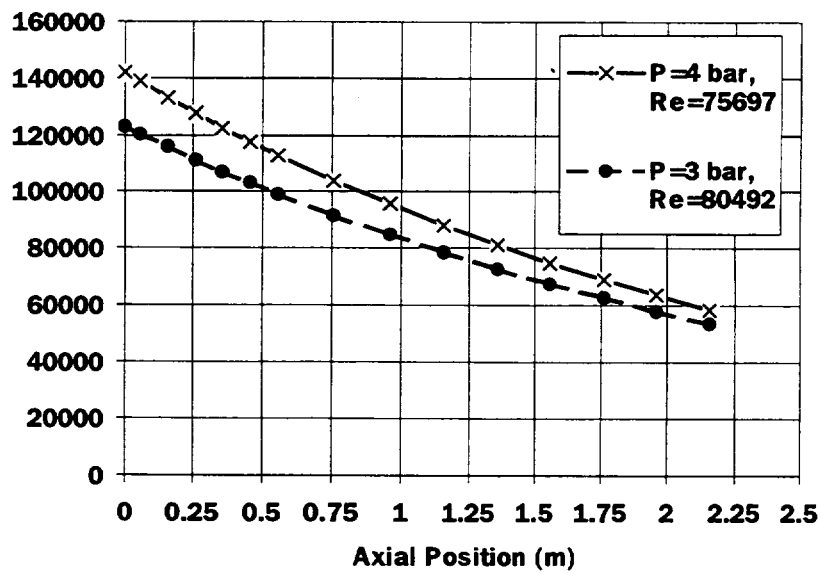


Figure 6.14. Effect of System Pressure (Air/Steam Mixture; X<sub>i</sub>=20 %)

Total of 9 experiments were repeated by zero inlet superheating degree, as described in Chapter 4. From these nine cases, three of them belong to the pure steam cases and the rest of them are for air/steam mixture with different air inlet quality settings. The overall finding of this investigation reveals the fact that the inlet superheating of steam has no considerable effect on heat flux. A sample result for heat flux, corresponding to the case of  $P_n=4$  bars and  $X_i=10\%$ , is presented in Figures 6.15.

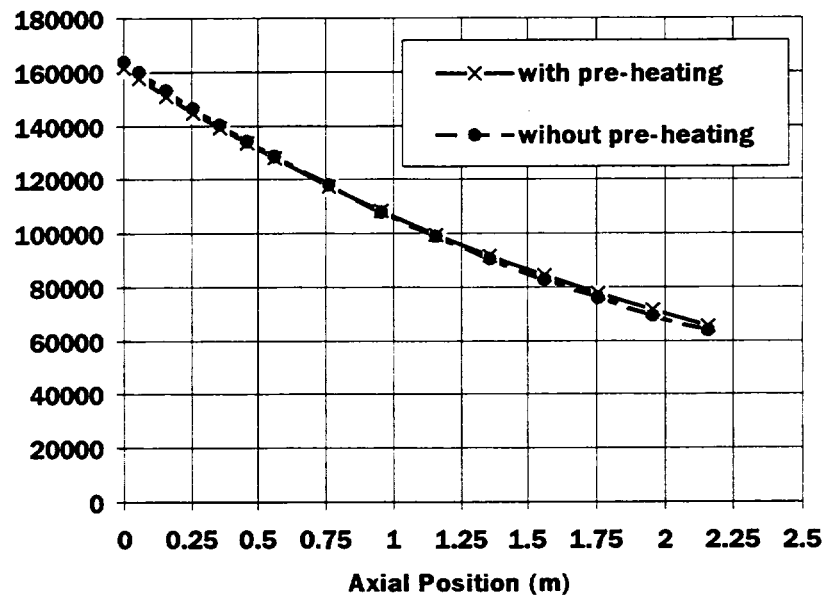


Figure 6.15. Effect of Inlet Superheating of Steam ( $P_n=4$  bars,  $X_i=10\%$ )

It should be pointed out that it is not surprising to have *no superheating effect* on local heat flux values since there is a subcooling at the centerline of condenser tube due to possible detachment of liquid droplets from the inner surface of tube. Hence, there is no considerable effect of dryness of steam at the entrance since it gets wetted throughout its flow in downward direction.

## 6.4 Local Air Mass Fraction Distribution

The local air mass fraction was predicted by using the data of predicted heat flux distribution. The local air mass fraction is defined as:

$$X_{air}(x) = \frac{\dot{m}_{air}}{\dot{m}_{air} + \dot{m}_v(x)} \quad (6.3)$$

To obtain the local air mass fraction (or air quality), the data for the local vapor mass flow rate changing along the channel due to condensation are needed. To calculate the local vapor mass flow rate, first the sectional condensate flow rate was obtained from a sectionwise steady state heat balance by neglecting the gas phase sensible heat transfer and considering only the latent heat transfer, which is given as

$$\Delta q = \Delta \dot{m}_{cond} h_{fg} \quad (6.4)$$

Here the latent heat of condensation ( $h_{fg}$ ) was calculated at the measured local inner wall temperature since film temperature is much closer to the inner wall temperature than that of bulk temperature. The local condensate flow rate, then, was calculated by summing up the incremental values up to that point. The local vapor mass flow rate was calculated by subtracting the local condensate mass flow rate from the known vapor flow rate measured at the inlet of the test section. Since the air mass flow rate is constant, Equation (6.3) can be used for determining the local air mass fraction.

The predicted data for the air mass fraction distribution along the channel helps us understand the trend of vapor mass flow rate that decreases towards the bottom of the channel, along with phase change due to condensation process. The predicted results of the air mass fraction are presented in Figures 6.16 and 6.17 which correspond to the system pressure of 2 bars and 4 bars, respectively.

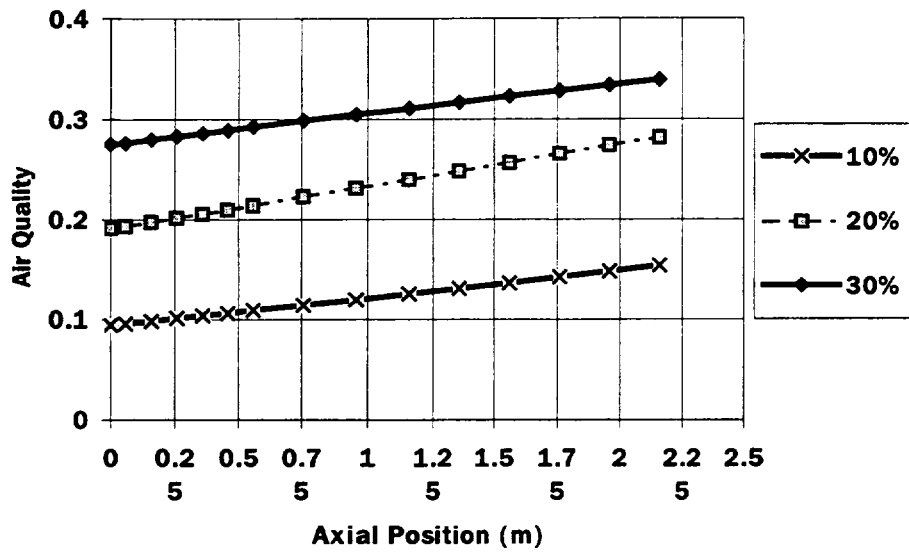


Figure 6.16. Distribution of Air Mass Fraction ( $P_n=2$  bars)

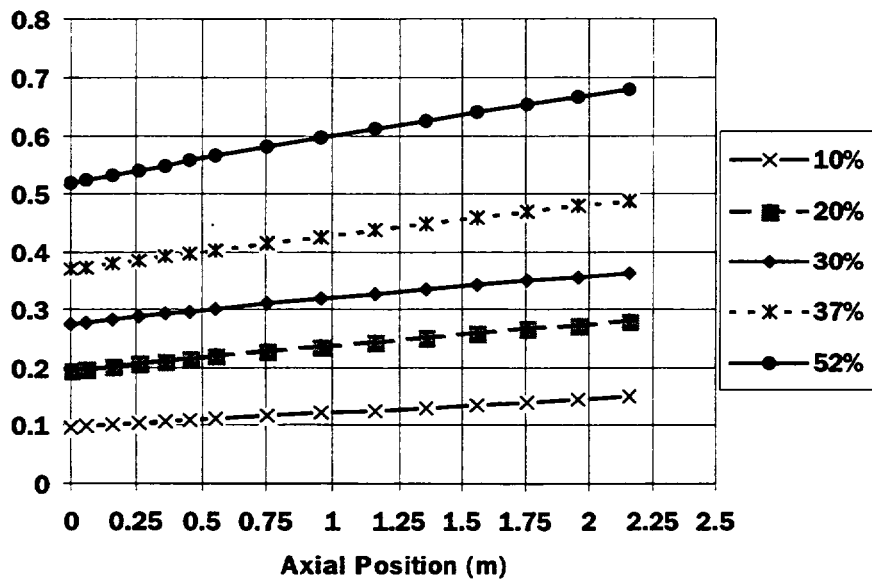


Figure 6.17. Distribution of Air Mass Fraction ( $P_n=4$  bars)

It is seen from the predicted data that the air mass fraction increases steadily along the channel as a result of condensate accumulation. This is known as “*suction effect*” since vapor-liquid phase change due to condensation sucks air towards the bottom of the test section. We can extract a general conclusion that the air quality is a linear function of the axial distance in spite of the heat flux behavior which exhibits an exponential trend.

### 6.5 Condensate Film Reynolds Number

When there is a sufficient amount of condensate flow, turbulence may appear in the condensate film which results in higher heat transfer rates. The criterion for determining whether the flow is laminar or turbulent is the Reynolds number, and for the condensation system it is defined as

$$\text{Re}_f = \frac{VD_h\rho_f}{\mu_f} = \frac{4AV\rho_f}{P\mu_f} \quad (6.5)$$

and by inserting  $P=\pi d$  for vertical tube, we get

$$\text{Re}_f = \frac{4\dot{m}_{cond}}{\pi d\mu_f} \quad (6.6)$$

where  $\dot{m}_{cond}$  is the mass flow rate through the particular section of the condensate film.

As the condensate layer thickness increases it can undergo a transition from laminar to turbulent flow. McAdams [10] suggests that transition could occur at a condensate Reynolds number of 1800 where the Reynolds number is defined in Eq. (6.5). At high values of the shear stress, however, Carpenter and Colburn found transition values as low as 200–300 [11]. Since Reynolds number of vapor is high (~54000–94000) in the experiments conducted at the METU-CTF, the later values of the condensate Reynolds number (200–300) are applicable for criteria of transition from laminar to turbulent flow. The sectional condensate flow rate was obtained from a sectionwise steady state heat balance and, then, the local condensate flow rate

( $\dot{m}_{cond}$ ) was calculated by summing up the incremental values up to that point. The local values of the condensate film Reynolds number were calculated and the results are presented in Figures 6.18 for system pressures of 2 bars. The calculated film Reynolds number decreases as air mass fraction increases at the same system pressure setting, and falls into the range of turbulent region for all experimental runs (other than those performed at a system pressure of about 1.5 bars), i.e.  $Re_f > 300$ . For example; the film Reynolds number increases up to about 3500 for pure vapor run performed at the nominal system pressure of 6 bars.

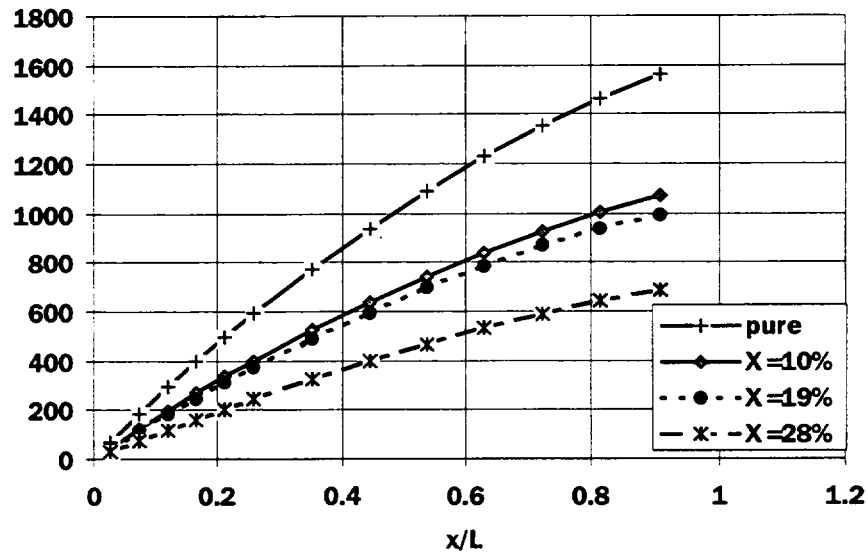


Figure 6.18. Distribution of Condensate Film Reynolds Number ( $P_n=2$  bars)

### 6.6. Comparison with Theory

A set of simulations was performed by using the RELAP5/mod-3.2.1.2 thermal-hydraulic system analysis computer code. The code solves six equations (mass, momentum, and energy) for two-phase and one equation (mass) for noncondensable gas. The heat transfer solution scheme of the code also includes condensation of water vapor containing noncondensable gas, such as air, hydrogen, nitrogen, helium. The RELAP5 code calculates a wall heat transfer coefficient based on condensation logic under the following conditions:

- The wall temperature is below the saturation temperature based on the bulk partial pressure of vapor calculated by using the Gibbs-Dalton ideal gas mixture equation.
- The liquid temperature is above the wall temperature.
- The liquid void fraction is greater than 0.1.
- The bulk noncondensable quality is less than 0.999.
- The pressure is below the critical pressure.
- Only filmwise condensation exists.

The default model used currently is the Shah-Colburn-Hougen model. The Shah model replaces the Nusselt model for pure steam condensation if the heat transfer coefficient calculated by this model is greater than that of Nusselt model. The Colburn-Hougen diffusion model, used for taking into account the inhibiting effect of a noncondensable gas, involves an iteration process to solve for the steam saturation temperature at the interface between the steam/gas boundary layer and water film. The model was developed under the following assumptions:

- The sensible heat transfer through the diffusion layer to the interface is negligible.
- Stratification of the gas in vapor by buoyancy effects is negligible.
- Required mass transfer coefficients can be obtained by applying the analogy between the heat and mass transfer.
- The gas is not removed from the vapor region by dissolving it in the condensate.

The formulation is based on the principle that the heat transferred by condensing vapor at liquid-vapor interface which is diffusing through the noncondensable gas is equal to the heat transfer through the condensate. This energy conservation principle, obviously, needs interface pressure (or temperature) to be determined since the interface pressure is always lower than the bulk pressure (total pressure) at the core due to existence of the noncondensable gas at the interface. One of the deficiency of the model is the assumption of having same gas and vapor velocities which is not necessarily correct in reality. Moreover, the effect of superheating of steam was not incorporated in the formulation.

Some of the experimental cases with air/steam mixture were simulated by the RELAP5/mod-3.2.1.2 beta test version by imposing the measured inner wall temperatures as boundary condition which means that the jacket pipe was not modelled for not to increase the uncertainty associated with the flow inside the jacket pipe. The results of heat flux predictions are plotted against the experimental data as given in Figure 6.19.

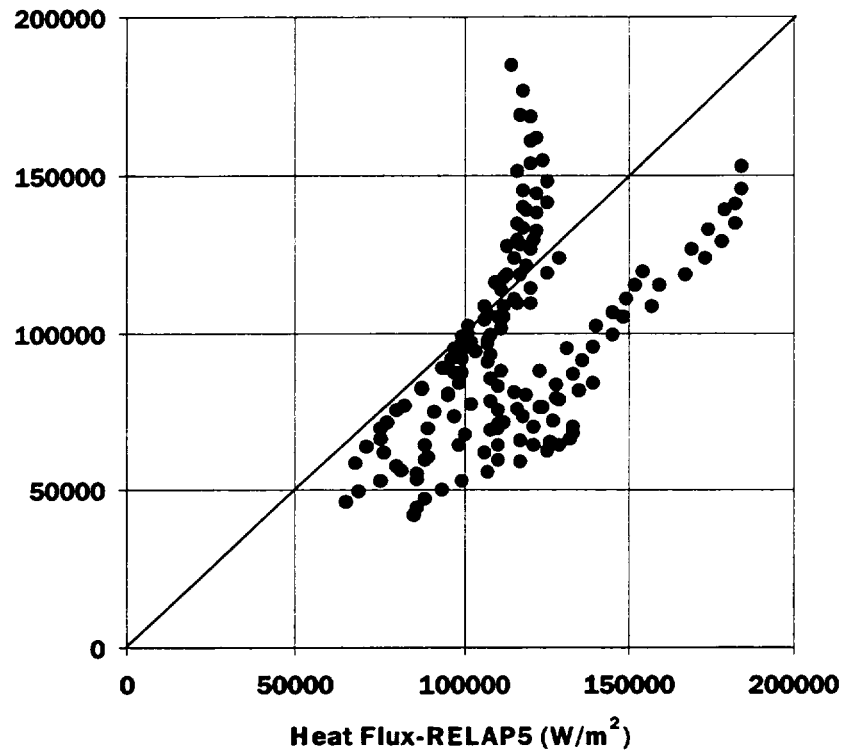


Figure 6.19. Comparison of Measured and Predicted Local Heat Flux Values

It is clear that the RELAP5 code overpredicted majority of experimental local heat flux data by 5 % – 50 %. In general, the deviation increases by increase of inlet air mass fraction.

## LIST OF REFERENCES

1. Tanrikut, A., Heper, H., Bayraktar, N. and Gunel, I., "The Simulation of Loss of Heat Residual System after Reactor Shutdown," Annual Meeting on Nuclear Technology '94, Stuttgart, 1994.
2. Tanrikut, A., "In-Tube Condensation in the Presence of Air," Ph.D. Thesis, Mechanical Engineering Department, Middle East Technical University, Ankara, 1998.
3. Tanrikut, A., "An Assessment of RELAP5 Code for Pure Steam Condensation and Condensation in the Presence of Air," Annual Meeting for Nuclear Technology, Mannheim (Germany), 21-24 May 1996.
4. RELAP5/MOD3 Code Manual, Code Structure, System Models and Solution Methods, Idaho National Engineering Laboratory, NUREG/CR-5535, Vol. 1, 1995.
5. Methods of Measurements of Fluid in Closed Conduits, British Standard Institution, BS-1042, Section 1.1, 1981.
6. Brinkworth, B. J., *An Introduction to Experimentation*, The English Universities Press Ltd., 1968.
7. Kuhn, S. Z., Schrock, V. E. and Peterson, P. F., "Final Report on U. C. Berkeley Single Tube Condensation Studies," Dept. of Nuclear Eng., UCB-NE-4201, 1994.
8. Siddique, M., Golay, M. W. and Kazimi, M. S., "The Effect of Noncondensable Gases on Steam Condensation under Forced Convection Conditions," Dept. of Nuclear Eng., MIT, MIT-ANP-TR-010, 1992.
9. Tanrikut, A., Yesin, O., "An Experimental Research on In-tube Condensation in the Presence of Air," 2<sup>nd</sup> International Symposium on Two-phase Flow and Experimentation, Pisa (Italy), 23-26 May 1999.
10. W. H. McAdams, *Heat Transmission*, McGraw-Hill Book Company, Inc., New York, 1954.
11. W. H. Rohsenow, J. H. Webber and A. T. Ling, Effect of Vapor Velocity on Laminar and Turbulent Film Condensation, *Trans. ASME*, Vol. 78, 1956.

APPENDIX A

PHOTOGRAPHS OF THE METU-CTF

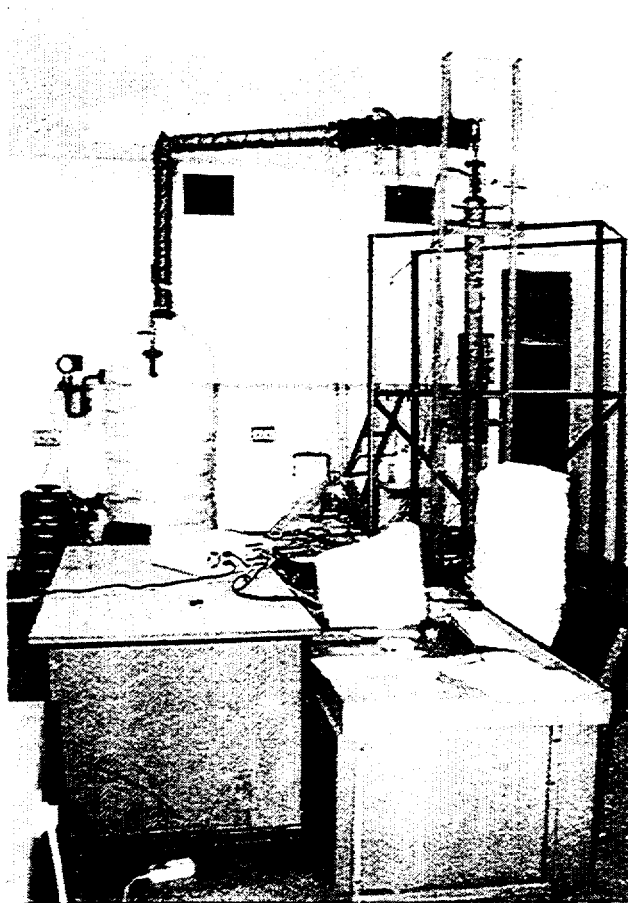


Figure A.1. General View of the METU-CTF

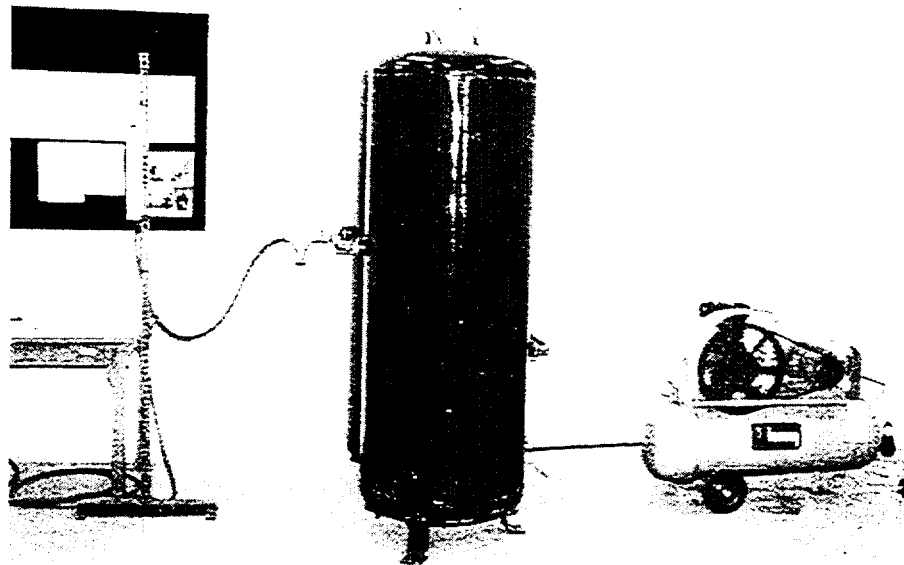


Figure A.2. The Compressed Air Supply System

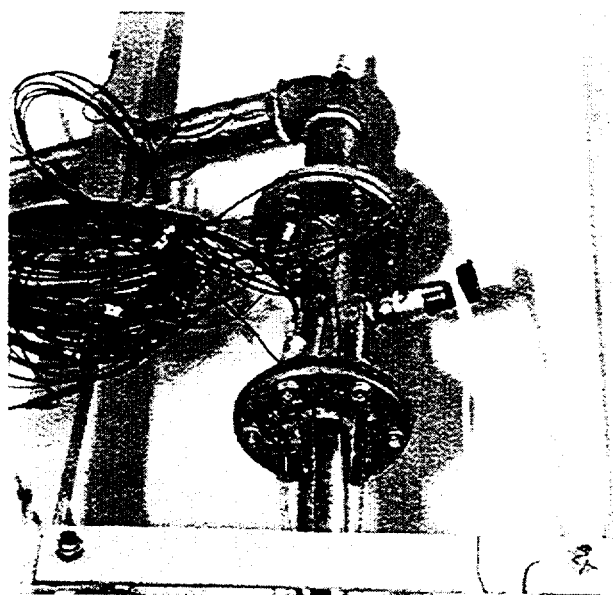


Figure A.3. The Upper Part of the Test Section (without the Jacket Pipe)

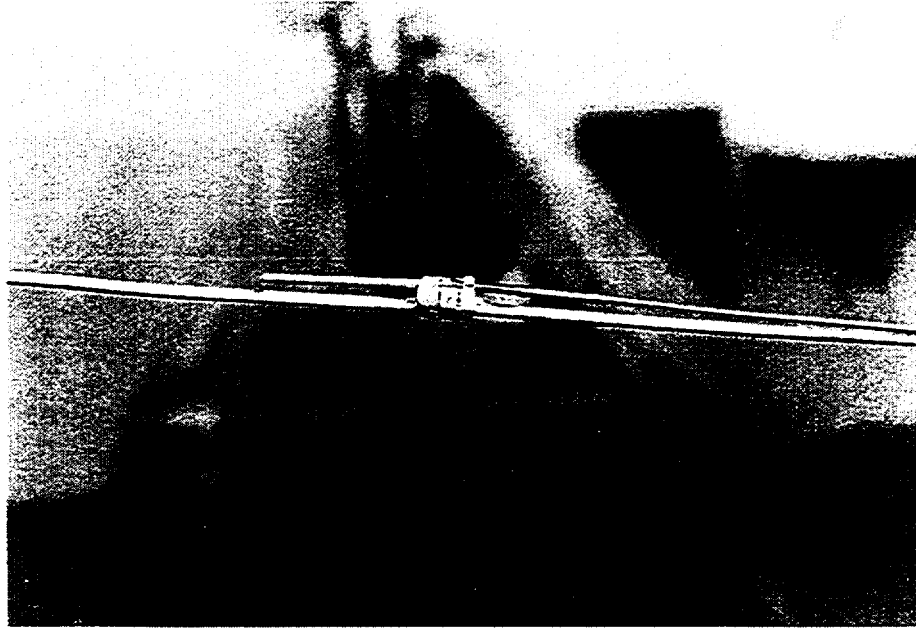


Figure A.4. The Thermocouple (D=1.5 mm) Fixed to the Guide Wire (D=2 mm) to be Placed Inside the Condenser Tube for Central Temperature Measurement



Figure A.5. The Thermocouple (D=1.5 mm) Fixed Inside the Condenser Tube for Inner Wall Temperature Measurement

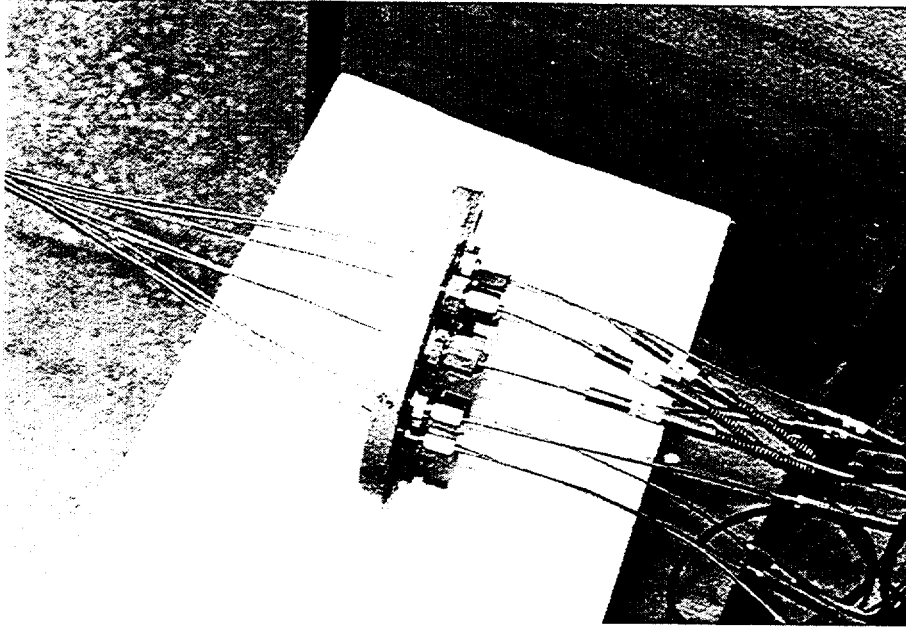


Figure A.6. The Lower Flange of Test Section and Penetration of Thermocouples Used for Central Temperature Measurement

## APPENDIX B

### SPECIFICATIONS OF INSTRUMENTATION AND DATA ACQUISITION SYSTEMS

#### 1) Thermocouples:

Manufacturer: ELIMKO Co., Turkey  
Type: L (Fe-Const type designed according to German DIN standard)  
J (Fe-Const type designed according to USA standard)

Class: 2  
Temperature Range:  $-40\text{ }^{\circ}\text{C}$  to  $333\text{ }^{\circ}\text{C}$   
Tolerance Value:  $\pm 2.5\text{ }^{\circ}\text{C}$  according to the standard IEC 584-2

#### 2) Pressure Transducer:

Manufacturer: Transinstruments Inc., England  
Type: Strain gauge  
Working Medium: Water, steam, gas  
Pressure Range: 0–6 bar (g)  
Output Signal: 4–20 mA (linear)

#### 3) Flowmeter:

Manufacturer: ABB Kent-Taylor, Italy  
Type: Differential pressure transmitter  
Working Medium: Water, steam, gas  
dP Range: 11.7–70 kPa  
Output Signal: 4–20 mA (linear)

#### 4) Data Acquisition System:

Manufacturer: Advantech Co., Ltd.  
Data Acquisition Card: PCL-812PG  
Analog Input: 16 single-ended channels  
12 bits resolution  
 $\pm 5\text{V}$ ,  $\pm 2.5\text{V}$ ,  $\pm 1.25\text{V}$ ,  $\pm 0.625\text{V}$ , and  $\pm 0.3125\text{V}$  input range  
0.015% of reading  $\pm 1$  bit accuracy  
Analog Output: 2 channels  
12 bits resolution  
Amplifier/Multiplexer Board: PCLD-889  
Input Channel: 16  
Input Range:  $\pm 10\text{V}$  maximum  
Cold Junction Compensation:  $+24.4\text{V}/^{\circ}\text{C}$   
0.0V at  $0.0\text{ }^{\circ}\text{C}$

## APPENDIX C

### ERROR ANALYSIS

The total error of a function F with independent measured variables  $x_1, x_2, x_3, \dots, x_n$ , was obtained as [6]:

$$\sigma_F = \left[ \left( \frac{\partial F}{\partial x_1} \sigma_{x_1} \right)^2 + \left( \frac{\partial F}{\partial x_2} \sigma_{x_2} \right)^2 + \dots + \left( \frac{\partial F}{\partial x_n} \sigma_{x_n} \right)^2 \right]^{1/2} \quad (C.1)$$

The relative error can be found by dividing the expression given above by F:

$$\frac{\sigma_F}{F} = \left[ \left( \frac{\sigma_{x_1}}{x_1} \right)^2 + \left( \frac{\sigma_{x_2}}{x_2} \right)^2 + \dots + \left( \frac{\sigma_{x_n}}{x_n} \right)^2 \right]^{1/2} \quad (C.2)$$

The experimental heat flux is defined as:

$$q''(x) = -\frac{\dot{m}_{cw} c_p}{\pi d_i} \frac{dT_{cw}(x)}{dx} \quad (C.3)$$

Therefore:

$$\frac{\partial q''}{\partial \dot{m}_{cw}} = -\frac{c_p}{\pi d_i} \frac{dT_{cw}(x)}{dx} \quad (C.4)$$

$$\frac{\partial q''}{\partial (dT_{cw} / dx)} = -\frac{\dot{m}_{cw} c_p}{\pi d} \quad (C.5)$$

Substituting Equations (C.4) and (C.5) into Equation (C.1) and dividing both sides of by  $(q'')^2$  we find the relative error for  $q''$ :

$$\frac{\sigma_{q''}}{q''} = \left[ \left( \frac{\sigma_{\dot{m}_{cw}}}{\dot{m}_{cw}} \right)^2 + \left( \frac{\sigma_{(dT_{cw}/dx)}}{dT_{cw}(x)/dx} \right)^2 \right]^{1/2} \quad (C.6)$$

The variables  $c_p$ , and  $d$  are assumed to be error free.

Similarly, the relative error for the condensation heat transfer coefficient is found from the following equation:

$$h_{exp}(x) = \frac{q''(x)}{(T_s(x) - T_w(x))} \quad (C.7)$$

The relative error for  $h_{exp}$  is:

$$\frac{\sigma_{h_{exp}}}{h_{exp}} = \left[ \left( \frac{\sigma_{q''}}{q''} \right)^2 + \left( \frac{\sigma_{(T_s - T_w)}}{(T_s - T_w)} \right)^2 \right]^{1/2} \quad (C.8)$$

Since we did not use a flow meter for cooling water flow measurement, the relative error for measured flow rate is taken from the maximum weight deviation calculated from the measurement performed in the beginning and end of each run. It is found that the maximum relative error associated with the cooling water measurement is 0.05, on the average, which corresponds to a deviation of 200 gr at the 4300 gr total weight of cooling water collected for a period of 15 s.

The slope of the coolant water axial temperature profile, i.e.  $dT_{cw}/dx$ , was determined from an exponential fit of the measured coolant temperatures as the function of the measurement distance, and for almost all the runs the  $R^2$  value for the fit of the data to the exponential relation was greater than 0.98. This means that error associated to the curve fitting is very small. However, it is difficult to predict the error associated with the temperature gradient directly. Only an estimation was made by considering the effect of measured temperature data with higher deviation than the general trend of the temperature distribution. It was found that the effect of measured temperature data with high deviation yields an error of  $\pm 10\%$ . The percent error of the temperature gradient assumed for the UCB-4 data was also  $\pm 10\%$  [7].

For the prediction of the uncertainty associated with the heat transfer coefficient, the standard deviation of the thermocouples must be known. The experimental data of isothermal check of thermocouples were used for determining the standard deviation of thermocouples. The experimental data, as given in Table 3.1, yields a maximum standard deviation of 0.762. Since this is an experimental result, the calculated standard deviation includes the tolerances given by the factory.

The aforementioned values of standard deviations and data needed for Equations (C.6) and (C.8) are summarized as follows:

$$\sigma_m = 0.05 m_{cw} \quad (C.9)$$

$$\sigma_{T_s} = \sigma_{T_w} = 0.762 \quad (C.10)$$

$$\sigma_{(dT/dx)} = 0.10 (dT_{cw}/dx) \quad (C.11)$$

$$(T_s - T_w) = 5 \text{ }^\circ\text{C} \quad (C.12)$$

$$\sigma(T_s - T_w) = (\sigma_{T_s}^2 + \sigma_{T_w}^2)^{1/2} \quad (C.13)$$

Substituting values from Equations (C.9) to (C.13) in Equations (C.6) and (C.8) we get:

$$\left[ \frac{\sigma_{q''}}{q''} \right]_{\max} = 0.11$$

and

$$\left[ \frac{\sigma_h}{h} \right]_{\max} = 0.24$$

Therefore the maximum uncertainties associated with the heat flux and the heat transfer coefficient are  $\pm 11\%$  and  $\pm 24\%$ , respectively. The temperature difference ( $T_s - T_w$ ) was equal to or greater than  $5\text{ }^\circ\text{C}$  in the major part of the condenser tube length in all experiments. However, this temperature difference is less than  $5\text{ }^\circ\text{C}$  in entrance region ( $-0.25\text{ m}$ ) and the uncertainty associated with the heat transfer coefficient escalates to  $\pm 38\%$  when a temperature difference of  $3\text{ }^\circ\text{C}$  is assumed. It is also observed that the error associated with the heat flux and the heat transfer coefficient increases when the coolant temperature change per unit length decreases which happens towards the end of the condenser tube. If we assume a conservative value for the deviation of the coolant temperature gradient such as  $15\%$  (instead of  $10\%$ ), the uncertainties become  $16\%$  and  $27\%$  for heat flux and heat transfer coefficient, respectively. This reveals that the uncertainty band increases at the entrance region much more than the end of the test section.

**BIBLIOGRAPHIC DATA SHEET**

*(See instructions on the reverse)*

1. REPORT NUMBER  
(Assigned by NRC, Add Vol., Supp., Rev.,  
and Addendum Numbers, if any.)

NUREG/IA-0184

2. TITLE AND SUBTITLE

In-Tube Steam Condensation in the Presence of Air

3. DATE REPORT PUBLISHED

MONTH	YEAR
June	2000

4. FIN OR GRANT NUMBER

5. AUTHOR(S)

A. Tanrikut, O. Yesin

6. TYPE OF REPORT

Technical

7. PERIOD COVERED *(Inclusive Dates)*

8. PERFORMING ORGANIZATION - NAME AND ADDRESS *(If NRC, provide Division, Office or Region, U.S. Nuclear Regulatory Commission, and mailing address; if contractor, provide name and mailing address.)*

Turkish Atomic Energy Authority  
Eskisehir Yolu  
06530 Ankara, Turkey

9. SPONSORING ORGANIZATION - NAME AND ADDRESS *(If NRC, type "Same as above"; if contractor, provide NRC Division, Office or Region, U.S. Nuclear Regulatory Commission, and mailing address.)*

Division of Systems Analysis and Regulatory Effectiveness  
Office of Nuclear Regulatory Research  
U.S. Nuclear Regulatory Commission  
Washington, DC 20555-0001

10. SUPPLEMENTARY NOTES

11. ABSTRACT *(200 words or less)*

In this research work, in-tube condensation in the presence of air is investigated experimentally for different operating conditions, and inhibiting effect of air is analyzed by comparing the experimental data of air/steam mixture with the data of corresponding pure steam cases, with respect to temperature, heat flux, air masses fraction, and film Reynolds number. The test matrix covers the range of:  $P_n=2-6$  bars,  $Re_v=45,000-94,000$ , and  $X_i+0\% - 52\%$ . The inhibiting effect of air manifests itself as a remarkable decrease in centerline temperature (10 oC - 50 oC), depending on inlet air mass fraction. However, the measured centerline temperature is suppressed compared to the predicted one, from the Gibbs-Dalton law, which indicated that the centerline temperature measurements are highly affected by inner wall thermal conditions, possibly due to narrow channel and high vapor Reynolds number.

12. KEY WORDS/DESCRIPTORS *(List words or phrases that will assist researchers in locating the report.)*

Condensation  
Noncondensables

13. AVAILABILITY STATEMENT

unlimited

14. SECURITY CLASSIFICATION

*(This Page)*

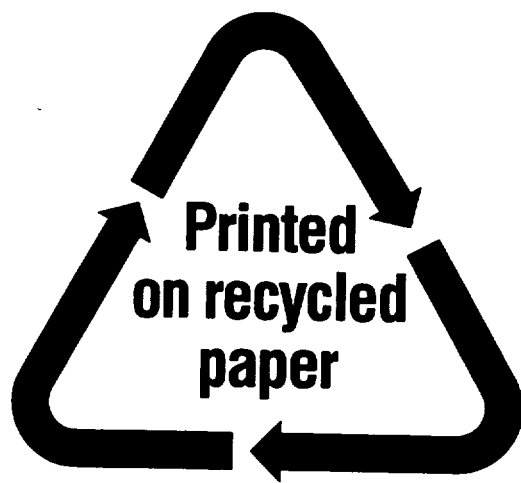
unclassified

*(This Report)*

unclassified

15. NUMBER OF PAGES

16. PRICE



Federal Recycling Program

**UNITED STATES  
NUCLEAR REGULATORY COMMISSION**  
WASHINGTON, D.C. 20555-0001

